atmosphere

Article

Impact of NO_x and NH_3 Emission Reduction on Particulate Matter across Po Valley: A LIFE-IP-PREPAIR Study

Giorgio Veratti [1,2,*], Michele Stortini [2], Roberta Amorati [2], Lidia Bressan [2], Giulia Giovannini [2], Stefano Bande [3], Francesca Bissardella [3], Stefania Ghigo [3], Elisabetta Angelino [4], Loris Colombo [4], Giuseppe Fossati [4], Giulia Malvestiti [4], Alessandro Marongiu [4], Alberto Dalla Fontana [5], Barbara Intini [5] and Silvia Pillon [5]

1 Department of Engineering "Enzo Ferrari", University of Modena and Reggio Emilia, 41125 Modena, Italy
2 ARPAE Emilia-Romagna, Regional Environmental Agency of Emilia-Romagna, 40122 Bologna, Italy; mstortini@arpae.it (M.S.); ramorati@arpae.it (R.A.); lbressan@arpae.it (L.B.)
3 ARPA Piemonte, Regional Environmental Agency of Piemonte, 10135 Torino, Italy; stefano.bande@arpa.piemonte.it (S.B.); franbiss@arpa.piemonte.it (F.B.); stefghig@arpa.piemonte.it (S.G.)
4 ARPA Lombardia, Regional Environmental Agency of Lombardia, 20162 Milano, Italy; e.angelino@arpalombardia.it (E.A.); lo.colombo@arpalombardia.it (L.C.); g.fossati@arpalombardia.it (G.F.); g.malvestiti@arpalombardia.it (G.M.); a.marongiu@arpalombardia.it (A.M.)
5 ARPA Veneto, Regional Environmental Agency of Veneto, 35121 Padova, Italy; alberto.dallafontana@arpa.veneto.it (A.D.F.); barbara.intini@arpa.veneto.it (B.I.)
* Correspondence: giorgio.veratti@unimore.it

Abstract: Air quality in Europe continues to remain poor in many areas, with regulation limits often exceeded by many countries. The EU Life-IP PREPAIR Project, involving administrations and environmental protection agencies of eight regions and three municipalities in Northern Italy and Slovenia, was designed to support the implementation of the regional air quality plans in the Po Valley, one of the most critical areas in Europe in terms of pollution levels. In this study, four air quality modelling systems, based on three chemical transport models (CHIMERE, FARM and CAMx) were applied over the Po Valley to assess the sensitivity of $PM_{2.5}$ concentrations to NO_x and NH_3 emission reductions. These two precursors were reduced (individually and simultaneously) from 25% up to 75% for a total of 10 scenarios, aimed at identifying the most efficient emission reduction strategies and to assess the non-linear response of $PM_{2.5}$ concentrations to precursor changes. The multi-model analysis shows that reductions across multiple emission sectors are necessary to achieve optimal results. In addition, the analysis of non-linearities revealed that during the cold season, the efficiency of $PM_{2.5}$ abatement tends to increase by increasing the emission reductions, while during summertime, the same efficiency remains almost constant, or slightly decreases towards higher reduction strengths. Since the concentrations of $PM_{2.5}$ are greater in winter than in summer, it is reasonable to infer that significant emission reductions should be planned to maximise reduction effectiveness.

Keywords: emission scenarios; NH_3; NO_x; $PM_{2.5}$; CTM; Potential Impacts (PI); Po Valley

check for updates

Citation: Veratti, G.; Stortini, M.; Amorati, R.; Bressan, L.; Giovannini, G.; Bande, S.; Bissardella, F.; Ghigo, S.; Angelino, E.; Colombo, L.; et al. Impact of NO_x and NH_3 Emission Reduction on Particulate Matter across Po Valley: A LIFE-IP-PREPAIR Study. *Atmosphere* **2023**, *14*, 762. https://doi.org/10.3390/atmos14050762

Academic Editor: James Lee

Received: 14 March 2023
Revised: 16 April 2023
Accepted: 18 April 2023
Published: 22 April 2023

1. Introduction

The scientific community has overwhelmingly demonstrated that particulate matter has harmful impacts on human health [1–5]. In particular, long-term exposure to fine particulate matter concentrations ($PM_{2.5}$) has been associated with cardiovascular, neurological and respiratory diseases as well as with cancer and mortality [6–9]. Acute exposure to $PM_{2.5}$ is also linked to detrimental health impacts, such as cardiovascular and respiratory disorders, diabetes, neurological diseases and deep vein thrombosis [10–13]. Despite the fact that mitigation measures have decreased pollution levels in several nations, air quality levels in some parts of Europe are beyond the most recent WHO recommendations [14] and the limit values specified in the EU air quality regulations [15]. This is particularly true for $PM_{2.5}$ concentrations, for which many urban areas, especially those in Northern Italy (Po Valley) and Eastern Europe (Poland, Bosnia and Herzegovina, Kosovo, Croatia and Turkey), exceed the EU's yearly average limit value of 25 μg m^{-3} [15]. In addition, in 2020, all the EU-27 countries, apart from Estonia, measured $PM_{2.5}$ concentrations above the WHO daily and annual objectives of 15 and 5 μg m^{-3}.

To effectively reduce pollutant concentrations below exceedance levels, efficient and coordinated air quality solutions must be implemented and achieved. To meet this need, the EU Life-IP PREPAIR Project was designed to support the implementation of the regional air quality plans in the Po Valley, one of the most critical areas of Europe for pollution levels. Within the PREPAIR Project, the environmental agencies and the administrations of eight regions and three municipalities of Northern Italy and Slovenia have worked together to implement short- and long-term measures to abate pollution emissions and improve the air quality in the whole Po Valley [16].

The Po Valley is a well-known characteristic area of Europe where meteorological conditions favour the accumulation of pollutants: its climate is prone to air mass stagnation, characterised by low wind speed regimes and prolonged thermal inversion that can last for several days during the winter. In addition, characteristic processes for the formation of particulate matter make the secondary fraction account for the great majority (more than 50%) of the total $PM_{2.5}$ concentrations, as shown by many studies [17–22]. Although other regions of Europe experience similar shares of secondary fractions of total PM (e.g., south of Poland [23], England [24,25], Greater Paris region [26] and other areas of France [27]), the Po Valley is a peculiar site where non-linear processes (i.e., the non-linear response of pollutant concentrations to an emission change) [28–30] and large variations in seasonal and spatial chemical regimes occur [31,32]. Still today, chemical regimes and secondary particle processes remain partly unknown; however, clear is the role of nitrogen oxides and ammonia as $PM_{2.5}$ precursors. For all these reasons, the design and application of effective air quality plans is a challenging task, which requires a careful study of the atmospheric response to emissions changes.

Chemical transport models (CTMs) are numerical models that compute diffusion, transport and photochemical processes in the atmosphere, and they can be used to infer the pollutant concentrations to precursor changes by computing the effects of different hypothetical policies on air quality.

Recently, two works in the literature [31,32] have simulated emission reduction scenarios of inorganic precursors of $PM_{2.5}$ over the Po Valley, using a single-defined chemical transport model (EMEP). This study tackles the same topic: four different air quality (AQ) modelling systems were applied over the Po Valley to assess the effects of nitrogen oxide (NOx) and ammonia (NH3) reductions on $PM_{2.5}$ concentrations. Precursor changes are imposed as emission reductions of 25%, 50% and 75%, as in [31,32].

The AQ modelling systems are based on three different CTMs, namely CHIMERE [33,34], the Flexible Air quality Regional Model (FARM) [35,36] and the Comprehensive Air Quality Model (CAMx) [37–39]. This multi-model approach reduces the uncertainties intrinsically present in a singular CTM and increases the robustness of the results. In addition, all the AQ modelling systems have implemented a common emission dataset [40] with higher spatial resolution in comparison to [31,32].

The main goals of this paper are as follows:

1. To perform a multi-model sensitivity assessment of $PM_{2.5}$ concentrations to the inorganic precursor (NO_x and NH_3);
2. To investigate spatial and temporal variabilities of the chemical regimes over the Po Valley by considering two seasons, October–March and April–September (including the transition periods that are disregarded in [31,32]). The choice of the two periods follows the time cycle of the regional air quality plans, which impose structural and emergency measures for the period from October to March;
3. To analyse the non-linear response of the atmosphere considering different levels of emission reduction.

The structure of the paper is organised as follows. In Section 2, we describe the four AQ modelling systems, the emission inventory common to all the models and the emissions scenarios that are the focus of this study. In the same section, we also describe the potential impact, a useful indicator used for the discussion of results and to compare results with [31,32]. Section 3 presents the analysis of the base case concentrations, the impact of NO_x and NH_3 reductions, and the assessment of non-linearity in $PM_{2.5}$ concentrations with respect to precursor changes. In Section 4, we finally discuss the results, considering the main differences and the analogies compared to previous works [31,32].

2. Materials and Methods

2.1. Chemical Transport Models

Among all the air quality forecast tools operating on a daily basis within the PREPAIR project, four AQ modelling systems were selected for this study: NINFA-ER ("Network dell'Italia del Nord per previsioni di smog Fotochimico e Aerosol" [41], run by Arpae Emilia-Romagna), PieAMS ("Piemonte Atmospheric Modeling System", run by ARPA Piemonte), SMAL-LO ("System Modeling Air Lombardy", run by ARPA Lombardia) and SPIAIR ("*Sistema Previsione Inquinamento* Air", run by ARPAV) (see Figure 1 for the application domain of the four AQ modelling systems). They rely on three state-of-the-art CTMs, namely CHIMERE for NINFA-ER, FARM for PieAMS and SMAL-LO, and CAMx for SPIAIR. The AQ modelling systems share the same annual anthropogenic emission inventory for the whole Po Valley, but differ in terms of emissions spatialisation and speciation/disaggregation, application domain and grid, meteorological input and parameterisations, and gas-phase and aerosol mechanisms. The physical and chemical parameterisations included in each modelling system, together with the domain characteristics, are reported in Table 1.

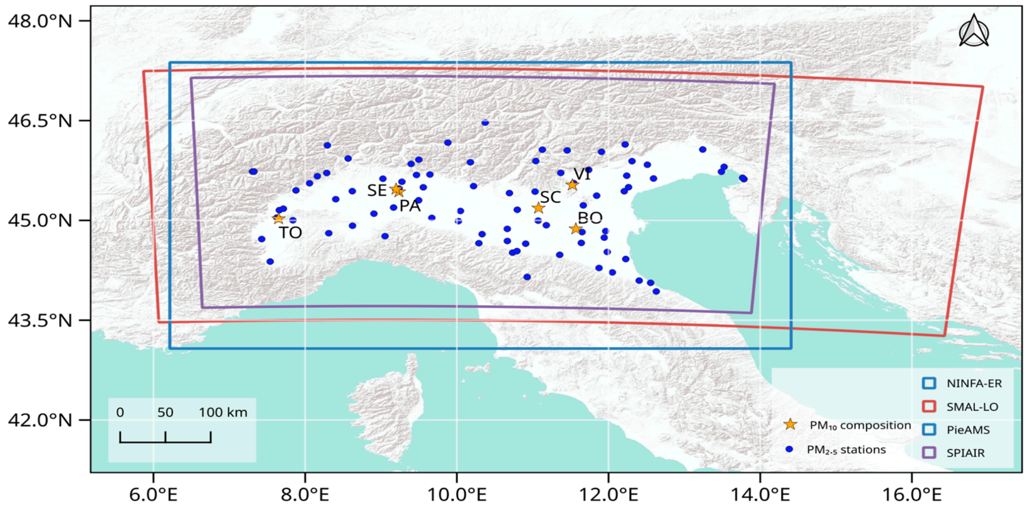

Figure 1. Computational domains of the AQ modelling systems. The background stations used for validation are indicated by blue dots, while orange stars show the super-site stations for PM_{10} composition. The NINFA-ER and PieAMS domains overlap.

The main differences concern gas-phase chemistry, aerosol models and meteorological drivers, which are briefly described below. The emission inventory and modules are discussed in Section 2.2.

The gas-phase chemical mechanisms are MELCHIOR2 [42] by NINFA-ER, SAPRC-99 POPS-Hg [43] by PieAMS and SMAL-LO, and the Carbon Bond mechanism (CB05, [44]) by SPIAIR. The MELCHIOR2 gas-phase scheme, implemented within the CHIMERE model, describes 120 chemical reactions of more than 40 gaseous species [45–47], while the SAPRC-99POPS-Hg (an updated version of SAPRC-99) includes 215 chemical reactions of more than 140 species. The CB05 mechanism, used by CAMx, describes 156 reactions of 51 species and it includes the simulation of hydrogen peroxide under low NO_x conditions.

The main difference in aerosol schemes is how each module manages the size distribution of the aerosol. The CHIMERE model simulates the main aerosol processes by dividing the aerosols in 10 size bins. PieAMS implements FARM with the AERO3_NEW [48] aerosol module, while SMAL-LO runs FARM with the AERO0 [49] aerosol module. The AERO3_NEW module describes particles distribution by a superposition of three lognormal distributions (Whitby approach [50]), while the AERO0 module and CAMx (SPIAIR) model use two size fractions for aerosols (fine and coarse).

Meteorological inputs for NINFA-ER, PieAMS and SPIAIR are provided by the limited area atmospheric model COSMO-5M, which is used every day by the Italian National Civil Protection Department (DPCM) and is implemented and operated by Arpae in the framework of the COnsortium for Small-scale MOdelling (http://www.cosmo-model.org/content/model/cosmo/default.htm, accessed on 2 March 2023) [51,52]. COSMO-5M covers the Mediterranean area with 5 km horizontal resolution and 45 vertical levels from 20 m up to 22 km. Conversely, the SMAL-LO model uses the Weather Research and Forecasting (WRF) model, version 4.1.1 [53], at 4 km horizontal resolution with 33 levels from 20 m up to 20 km.

The parameterisation of turbulent and convective processes in the atmosphere has a significant impact on atmospheric stability and, consequently, on the simulated chemical concentrations, as widely demonstrated by many studies [54–57]. For this reason, many schemes have been developed by different authors and each modelling system implements its own computational method. In this work:

- NINFA-ER accounts for the vertical turbulent mixing using the parameterisations of Troen and Mahrt [58], while the horizontal transport is simulated according to the formulation proposed by Van Leer [59];
- PieAMS and SMAL-LO make use of the vertical turbulence coefficients as implemented in the Random Displacement Method [60,61]. Horizontal diffusion coefficients are computed following the formulation of Smagorinsky [62] coefficients depending on the local stability class and the wind speed. Horizontal advection–diffusion operators are solved using the method by Yamartino [63], while the numerical integration of the vertical diffusion equation follows Yamartino et al. [64];
- SPIAIR accounts for vertical turbulent mixing by means of vertical diffusion coefficients [65]. Horizontal diffusion coefficients are determined within CAMx using a deformation approach based on the methods of Smagorinsky [62]. Horizontal advection is solved using the area preserving flux-form advection solver of Bott [66].

Table 1. Main features of the AQ modelling systems involved in this study.

	NINFA-ER	PieAMS	SMAL-LO	SPIAIR
CTM	CHIMERE2017 r4v1	FARM v4.13	FARM v4.13	CAMx v6.5
Operator	Arpae Emilia-Romagna	ARPA Piemonte	ARPA Lombardia	ARPA Veneto
Vertical layers	9 levels up to 5800 m a.s.l.	16 levels up to 7500 m a.s.l.	16 levels up to 7979 m a.s.l.	11 levels up to 6000 m a.s.l.
Depth of the first vertical layer	~25 m	10 m	20 m	20 m
Horizontal extension	Lon: 6.25–14.37° Lat: 43.1–47.35°	Lon: 6.25–14.37° Lat: 43.1–47.35°	Lon: ~6.0–16.7° Lat: ~43.4–47.2°	Lon: ~6.5–14.1° Lat: ~ 43.6–47.1°
Horizontal resolution	Lon: 0.07° Lat: 0.05°	Lon: 0.07° Lat: 0.05°	Lon: ~0.05° Lat: ~0.04°	Lon: ~0.05° Lat: ~0.04°
Meteorological driver	COSMO-5M model levels	COSMO-5M model levels	WRF-ARW	COSMO-5M pressure levels (from 1000 hPa to 300 hPa) and surface level (10 m)

Table 1. *Cont.*

	NINFA-ER	PieAMS	SMAL-LO	SPIAIR
Chemical boundary conditions	PREV'AIR	PREV'AIR	QualeAria forecast system	PREV'AIR
Advection scheme	Second-order van Leer scheme [59]	Finite elements method based on Blackman cubic polynomials [63]	Finite elements method based on Blackman cubic polynomials [63]	Horizontal advection uses input horizontal winds fields and is solved using the area preserving flux-form advection solver of Bott [66]
Vertical diffusion	Vertical diffusion coefficient (Kz) approach following Troen and Mahrt [58]	Vertical diffusion coefficient (Kz) approach following RDM model [60,61]. Hybrid semi-implicit/fully implicit scheme [64].	Vertical diffusion coefficient (Kz) approach following RDM model [60,61]. Hybrid semi-implicit/fully implicit scheme [64].	Kz approach, with vertical eddy diffusivity taken from CMAQ [65]
Gas-phase chemistry	MELCHIOR2	SAPRC-99_POPS-Hg	SAPRC-99_POPS-Hg	CB05
Aerosol model	10 bins (10 nm–40 µm)	AERO3_NEW [48]	AERO0 [49]	Coarse/Fine (CF)
Ammonium nitrate equilibrium	ISORROPIA II [67]	ISORROPIA II [68]	ISORROPIA II [68]	ISORROPIA [67]
SOA formation	Single-step oxidation scheme	SORGAM [69]	SORGAM [69]	SOAP [70]

2.2. Emission Inventory and Temporal Modulations

The LIFE PREPAIR project includes, among its products, a common air pollutant emission dataset on the Po Valley and Slovenia. The latest updated emission dataset refers to 2017 and has been extensively discussed in Marongiu et al. [40].

All the local emission inventories that have been used to compose the unitary PREPAIR inventory refer to the methodological reference EEA-EMEP Guidebook [71,72], and almost all use the same emission modelling system (INEMAR, [73]).

Figure 2 summarises the main results reported for the LIFE PREPAIR Emission dataset [40]. The combustion in the civil sector (mainly for heating) and road traffic are relevant sources of primary emissions of PM_{10}, CO and NO_x, while the agriculture sector, which encompasses manure management of livestock (housing, stocking and spreading) and the use of mineral fertilisers, is the main source of NH_3. Furthermore, residual content of sulphur in burned fuels in industrial sources is the primary source of SO_2.

Since the data regarding forest fires are collected at the municipal level but refer to different years, those emissions have been disregarded to avoid misleading results. Biogenic VOCs emissions were estimated for all AQ modelling systems with MEGAN (Model of Emissions of Gases and Aerosols from Nature [74]).

The emission density maps at the municipal level for primary PM_{10}, NO_x and NH_3 and additional detailed information can be found in [40].

The emission inventory adopted in this study distinguishes between stack sources and emissions produced near the ground; thus, all the AQ modelling systems account for both diffuse and point emission sources. Although all the modelling systems can allocate point sources at specific heights, each system adopts a different vertical distribution for diffuse emissions. More in detail, SPIAIR, due to a model limitation, sets all the diffusive emissions in the first model layer, i.e., between the ground and 20 m, while NINFA-ER, SMAL-LO and PieAMS distribute them following different vertical profiles according to the SNAP emission sector or activity.

Temporal and spatial patterns used to allocate annual emission inventory to hourly timestep are different for each modelling system. Figure 3 provides an overview of the temporal distribution of NH_3 emissions, a key precursor in the formation of secondary $PM_{2.5}$, throughout the year for each AQ modelling system. Figure 3a reports the total trimestral emissions and Figure 3b shows the monthly variability, providing the minimum and maximum monthly NH_3 emissions among the 4 models.

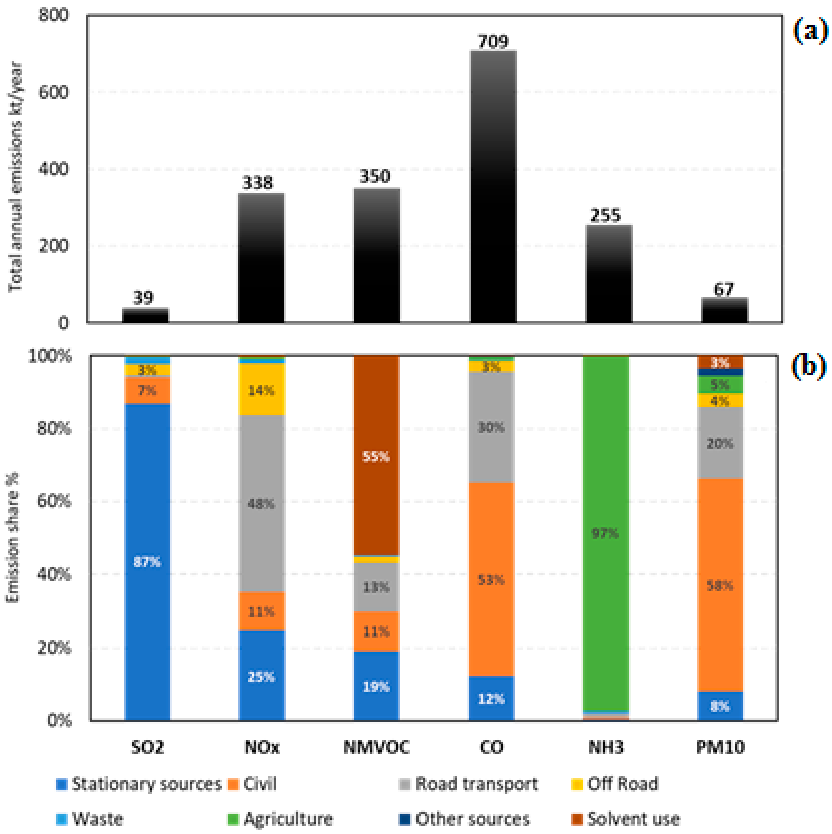

Figure 2. Total annual emissions on the Po Valley in kt year^{-1} (**a**) and their share by sector (**b**). Data do not contain the contribution of forest fires and biogenic sources.

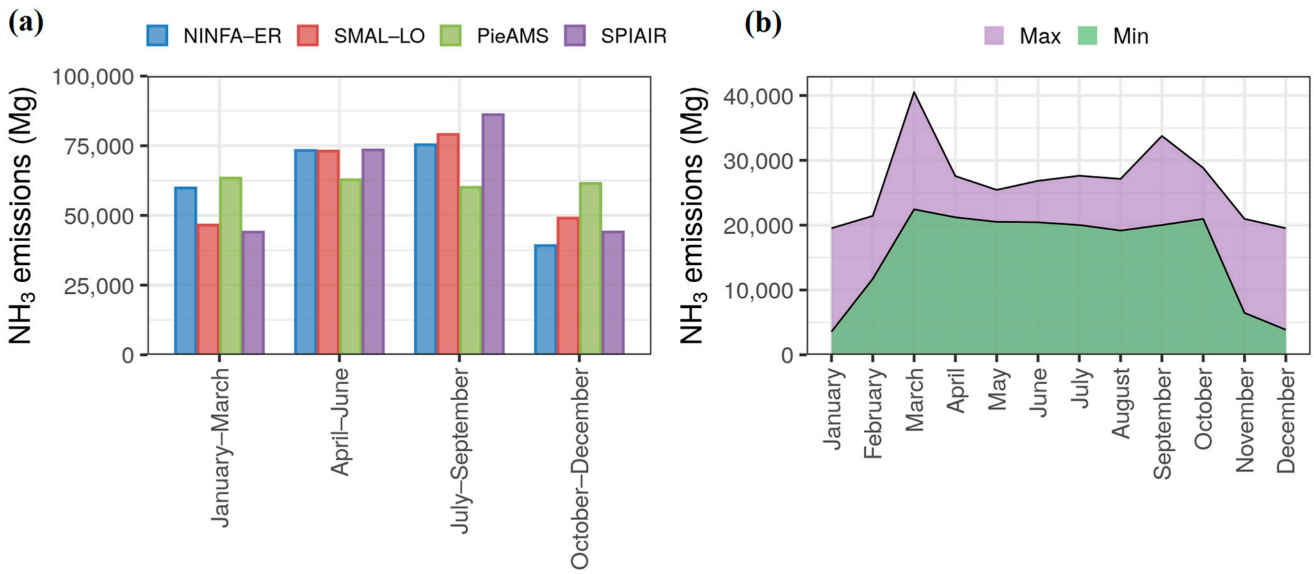

Figure 3. Total NH_3 emissions (**a**) and NH_3 monthly emissions variability of the AQ modelling systems (**b**).

2.3. Emission Scenarios

The reference year for meteorological conditions was 2019 and a total of ten emission scenarios were simulated using NINFA-ER, PieAMS, SMAL-LO and SPIAIR, as described in Table 2. The emission inventory outlined in Section 2.2 was used to simulate a base case scenario (named SC1), then NO_x and NH_3 precursors were reduced, either combined or individually, from 25% up to 75% for nine additional scenarios, as in Table 2, in the whole domain. No data assimilation was performed for any of the considered scenarios.

Table 2. Definition of the emission scenarios.

Reduction (%)	NO_x	NH_3	NO_x-NH_3
0		SC1 (base case)	
25	SC2	SC3	SC4
50	SC5	SC6	SC7
75	SC8	SC9	SC10

To study the impact of each emission reduction on concentrations, the results are focused on two main periods in 2019: a warm period from April to September and a cold period from October to March. In previous works [31,32], March and October are classified as transition periods and disregarded. In the present study, the entire year is considered by dividing it into two large seasons in order to compare results and explore similarities.

2.4. Indicators

Following the formulation already presented by [31,32], the effects of the emission reductions on $PM_{2.5}$ concentrations are analysed using the concept of potential impact. A potential impact (PI) is defined as a normalisation of the concentration changes (ΔC^{α}) with respect to the reduction strength (α). More specifically, ΔC^{α} can be computed as:

$$\Delta C^{\alpha} = PM2.5^{0} - PM2.5^{\alpha} \tag{1}$$

where $PM2.5^{0}$ represents the $PM_{2.5}$ concentration simulated using SC1, and $PM2.5^{\alpha}$ is the $PM_{2.5}$ concentration produced by an emission reduction α from SC1. Then, the PI of a single precursor is obtained as:

$$P^{\alpha}_{NH3} = \frac{\Delta C^{\alpha}_{NH3}}{\alpha},\ P^{\alpha}_{NOX} = \frac{\Delta C^{\alpha}_{NOx}}{\alpha} \tag{2}$$

When the simultaneous reduction in both precursors is performed, the total PI is the sum of the PI of the single precursors and a non-linear deviation term:

$$P^{\alpha}_{NOxNH3} = \frac{\Delta C^{\alpha}_{NH3}}{\alpha} + \frac{\Delta C^{\alpha}_{NOx}}{\alpha} + \frac{\hat{C}^{\alpha}_{NOxNH3}}{\alpha} = P^{\alpha}_{NH3} + P^{\alpha}_{NOx} + \hat{P}^{\alpha}_{NOxNH3} \tag{3}$$

$\hat{C}^{\alpha}_{NOxNH3}$ is the interaction term and it quantifies the non-linearities in $PM_{2.5}$ concentrations when an emission reduction is applied to both precursors (NO_x and NH_3).

Moving from an emission reduction α to a greater reduction β, it is possible to quantify the changes in the PI between the two considered reduction levels. Subtracting the α level PI from the β level PI, Equation (4) is obtained, and all the terms on the right side of this equation quantify the total non-linearity introduced moving from the emission reduction α to β. See [31,32] for further explanation.

$$P^{\beta}_{NOxNH3} - (P^{\alpha}_{NOX} + P^{\alpha}_{NH3}) = \hat{P}^{\alpha}_{NOxNH3} + \hat{P}^{\beta-\alpha}_{NOx} + \hat{P}^{\beta-\alpha}_{NH3} + \hat{P}^{\beta-\alpha}_{NOxNH3} \tag{4}$$

Generally, a limited number of scenarios are provided when designing air quality plans, and they are used to estimate the responses to other emission reduction levels. PIs could constitute effective formulations to determine the reduction threshold at which these responses remain proportional to each other and thus easy to interpret. In addition, PI can also be used to identify regions where the reduction in one of the precursors (on the whole domain) is more effective in mitigating pollutant concentrations.

In Section 3.3, two properties of PI are assessed to check the degree of linearity:

– Consistency, i.e., the variation in PI across the range of emission reductions;
– Additivity, i.e., the difference between the sum of the PI of each precursor and the PI resulting from the simultaneous reduction in all precursors.

3. Results

In this section, a preliminary description of the spatial and temporal variation in $PM_{2.5}$ concentrations is presented, and then modelled concentrations by the four modelling systems are validated against observations in terms of total daily $PM_{2.5}$ concentrations and daily PM_{10} inorganic components. Finally, chemical regimes and related non-linearities are analysed in the following sections by means of PI.

3.1. Base Case Concentrations and Model Validation

The base case is useful for model validation to verify whether the AQ models simulate the 2019 year satisfactorily, and for comparison with the scenarios of emission reduction.

The modelled $PM_{2.5}$ concentrations by NINFA-ER, PieAMS, SMAL-LO and SPIAIR are presented in Figure 4, where the average concentrations for the whole year are shown in the bottom panels, those for the winter period are shown in the central panels and those for the summer period are shown in the top panels. The winter season is characterised by the highest concentrations due to the typical Po Valley meteorological conditions: recurrent thermal inversions, persistent high-pressure systems and foggy conditions, which favour air mass stagnation and pollutant accumulation [17,75–79]. In addition, specific emission sources, such as non-industrial combustion processes, mainly wood burning for domestic heating, are relevant only during winter, exacerbating the accumulation of particulate matter in the whole Po Valley [80–82]. On the other hand, different weather conditions, such as convective processes induced by higher solar radiation reaching the land surface and lesser emissions, particularly those from domestic heating, favour generally better air quality during summertime.

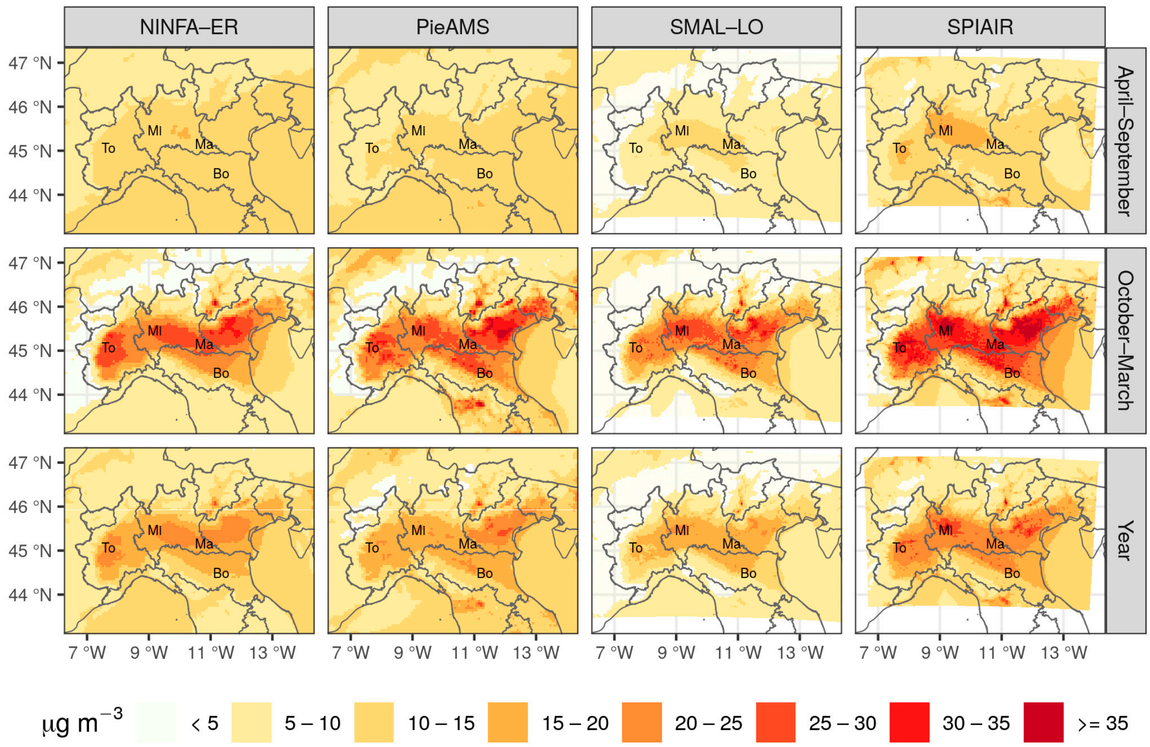

Figure 4. Maps of the average $PM_{2.5}$ concentrations for the period between April and September (top panels), between October and March (central panels) and for the whole year (bottom panels).

All four AQ systems reproduce very similar spatial patterns for the concentrations over the Po Valley (see Figure 4 and Table 3), with concentration averages differing by at most 5 μg m^{-3} for summer and winter periods, and by 4 μg m^{-3} for the yearly average. During wintertime, spatially averaged simulated $PM_{2.5}$ concentrations are between 10 and 15 μg m^{-3}. In this situation, SPIAIR tends to generally reproduce slightly higher values than the other three CTMs, possibly because anthropogenic diffusive emissions are all allocated to the first model layer, while the other systems account for more vertically spread out emissions, causing more diluted concentrations close to the ground. On the other hand, SMAL-LO shows generally slightly lower concentrations than the other systems, probably due to different boundary conditions which might impact total $PM_{2.5}$ concentrations all over the simulation domain.

Table 3. Statistics of spatial $PM_{2.5}$ concentrations for summertime ("Apr–Sep"), wintertime ("Oct–Mar") and yearly average ("Year") computed for available cells over the shared area by the four modelling systems.

Statistics	Period	NINFA-ER (μg m^{-3})	PieAMS (μg m^{-3})	SMAL-LO (μg m^{-3})	SPIAIR (μg m^{-3})
25th percentile	Apr–Sep	9	8	5	7
average	Apr–Sep	11	10	6	10
median	Apr–Sep	11	10	6	10
75th percentile	Apr–Sep	12	13	8	12
25th percentile	Oct–Mar	6	6	4	7
average	Oct–Mar	11	13	10	15
median	Oct–Mar	9	10	7	12
75th percentile	Oct–Mar	16	19	14	21
25th percentile	Year	8	7	4	7
average	Year	12	12	8	12
median	Year	11	11	7	11
75th percentile	Year	14	12	11	16

During spring and summertime, thanks to the increase in the atmospheric boundary layer depth and to high temperatures that favour the gas phase of semi-volatile compounds, $PM_{2.5}$ concentrations sharply decrease with respect to the winter period and average spatial concentrations fall to values between 7 and 11 μg m^{-3}, with very similar distribution over the whole domain (Figure 4).

The simulated $PM_{2.5}$ concentrations from SC1 were compared with measurements at 85 stations, located in rural, suburban and urban background areas within the Po Valley. In addition, PM_{10} chemical characterisation was performed at six urban background super-sites in Milan (Pascal and Senato stations, labelled as PA and SE, respectively, in Figure 1), Turin (TO), Bologna (BO) and Vicenza (VI) and at Schivenoglia (SC), a rural background location near Mantua. The PM_{10} components used for model comparison are those representative of inorganic aerosols, i.e., total nitrate and ammonium, since in this paper, only emission scenarios involving the reduction in those inorganic precursors are analysed. The effects of emissions reduction on the formation of secondary organic aerosols are not treated in this work. Figure 1 shows the station locations for total $PM_{2.5}$ and PM_{10} chemical composition.

The comparison results show that models' performances are in line with similar case studies focusing on the same area [57,83–85] (see Figure 5a for monthly time series and Figure 5b for model indicators). In addition, with the aim of assessing the models' capability to reproduce $PM_{2.5}$ concentrations for policy making purposes, the model error is compared with the Model Quality Objective (MQO) [86,87] using measurement uncertainty. The analysis outcomes show that the Model Quality Indicator (MQI), the statistical index used to determine whether the MQO is fulfilled, is lower than one for most of the stations (see Figure S1 in the Supplementary Materials). More specifically, the percentage of the stations that has the MQI lower than 1 for the yearly average $PM_{2.5}$ concentrations is between 95%

and 98%, depending on the model considered. This confirms that the model quality in reproducing $PM_{2.5}$ concentrations for policy use is fulfilled, and further investigations are based on a robust model performance.

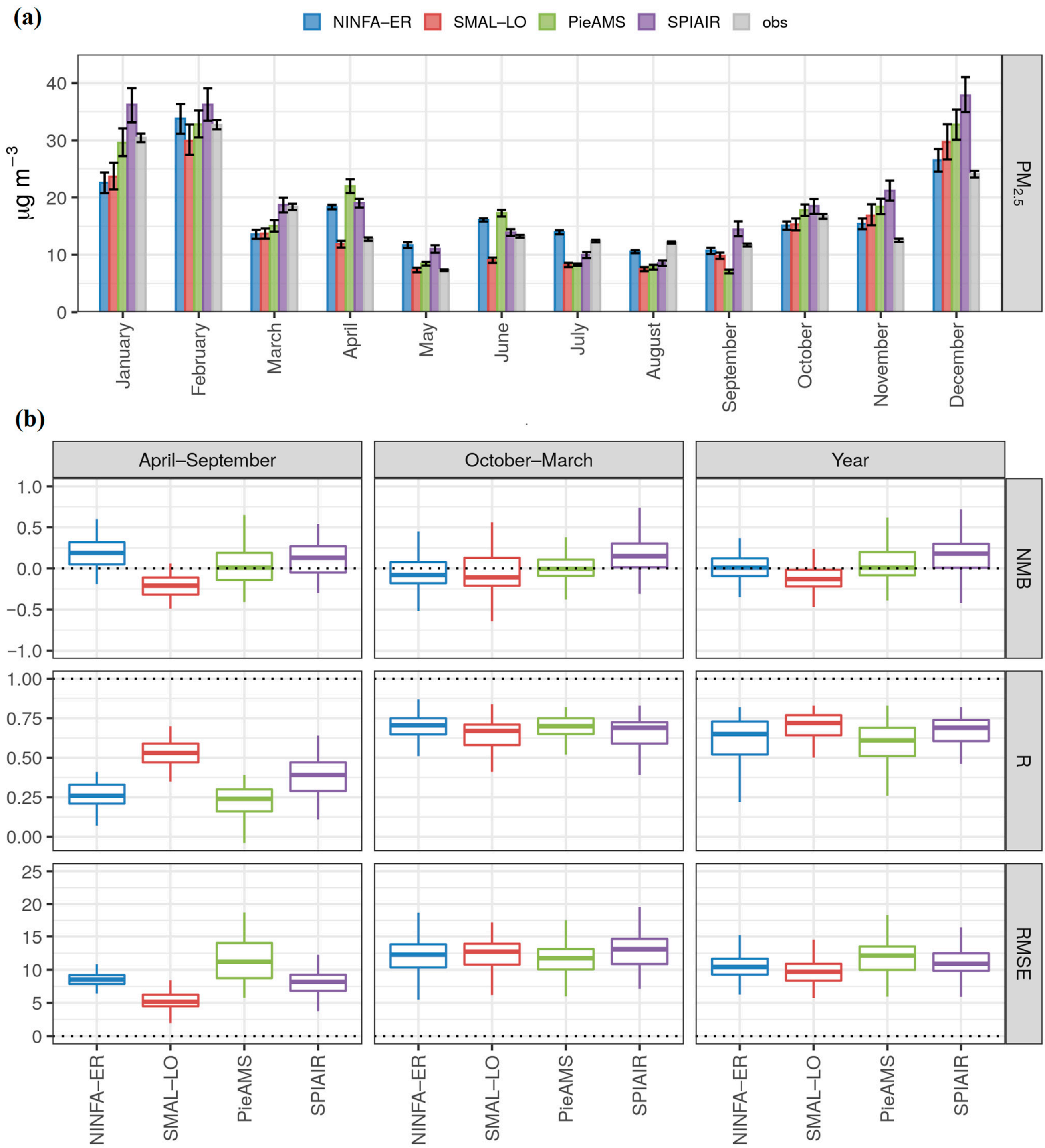

Figure 5. Comparison between modelled and observed monthly averaged $PM_{2.5}$ concentrations, with related 95% confidence intervals (black segments in (**a**)) and statistical scores for NMB, R and RMSE divided by season (**b**). The horizontal lines in a box indicate the median; the lower and upper ends of a box indicate the 25th and 75th percentiles, respectively.

Looking at the results more in detail (Figure 5b), SMAL-LO generally tends to underestimate observed $PM_{2.5}$ concentrations for both summertime and wintertime but expresses a higher Pearson correlation coefficient (R) with respect to other models for summer and yearly averages. NINFA-ER shows a contrasting behaviour between seasons: $PM_{2.5}$ observations are generally overestimated during summertime (particularly between April and July, Figure 5a) and underestimated during wintertime (mostly during January and March). PieAMS, despite higher root mean square error (RMSE) values for summertime with respect to other models, has an average normalised mean bias (NMB) very close to zero for both seasons and for the yearly average. On the other hand, SPIAIR generally tends to overestimate $PM_{2.5}$ observations during both wintertime and summertime, but RMSE and R are in line with the performances of the other models.

All the metrics previously mentioned are defined in Section S1 of the Supplementary Materials.

Figure S2 in the Supplementary Materials reports the mean modelled and observed concentrations of total nitrate (NO_3^-) and ammonium (NH_4^+) for all sites included in the analysis. Average concentrations and relative 95% confidence intervals are reported for summer and winter seasons, as well as for the yearly average. The results show that ammonium concentrations are generally overestimated by NINFA-ER, particularly at the rural background site (Schivenoglia), where the model failed to capture the yearly trend, probably due to an overestimation of the ammonia emissions in this area all throughout the year. The same model adequately reproduced total nitrate concentrations for all stations considered. SMAL-LO and PieAMS, probably because they rely on the same CTM, show generally similar results in reproducing total nitrate and ammonium concentrations, with the former being underestimated during wintertime and the latter being well reproduced throughout the whole year. Finally, SPIAIR, confirming the results obtained for the total $PM_{2.5}$ concentrations, generally slightly overestimates all the inorganic components considered in this study for the six stations.

3.2. Potential Impacts (PI) of Precursor Reduction

In previous studies [31,32], the Po Valley has been highlighted as one of the most heterogeneous areas in Europe in terms of chemical processes that lead to the formation of secondary inorganic aerosols, with contrasting chemical regimes being present within hundreds of kilometres. Here, four modelling systems, in combination with a detailed and updated emission inventory, were used to provide a detailed characterisation of chemical regimes across the Po Valley during the cold and warm seasons. Different meteorological forcing conditions and independent chemical schemes were used to provide a range of variability to models output, yielding an additional value with respect to previous works focusing on the same area.

As it is easy to prove, a combination of NO_x and NH_3 reductions is more effective than reducing one single precursor, unless there are strong non-linear negative interactions; nevertheless, it is worthwhile to assess which inorganic precursor needs to be prioritised to achieve greater $PM_{2.5}$ reductions. In this view, the individual PIs computed for the SC2, SC5 and SC8 scenarios are compared with PIs from SC3, SC6 and SC9. Figures 6 and 7 depict the spatial distribution of the difference $P^{\alpha}_{NOx} - P^{\alpha}_{NOx}$ for three levels of emission reduction (25%, 50% and 75%, reported in the first, second and third rows, respectively) during the cold (Figure 6) and warm (Figure 7) seasons. Positive values (red palettes) indicate areas where the reduction in NO_x will result in a greater reduction in $PM_{2.5}$ (also named NO_x-sensitive), and negative values (blue palettes) show the regions where NH_3 reductions are more effective in $PM_{2.5}$ abatement (NH_3-sensitive). Following previous studies, for very weak NO_x- or NH_3-sensitive regimes, i.e., for those areas where a reduction in one of the two precursors causes a close drop in $PM_{2.5}$ concentrations, a neutral regime, between -1 and $+1$ µg m^{-3}, is assumed. It is worth emphasising that defining NO_x- or NH_3-sensitive areas does not necessarily indicate that reducing emissions of NH_3 or NO_x, respectively, will have no effect on $PM_{2.5}$ concentrations. Rather, the relative magnitude of its effects is smaller compared to reducing the other precursor.

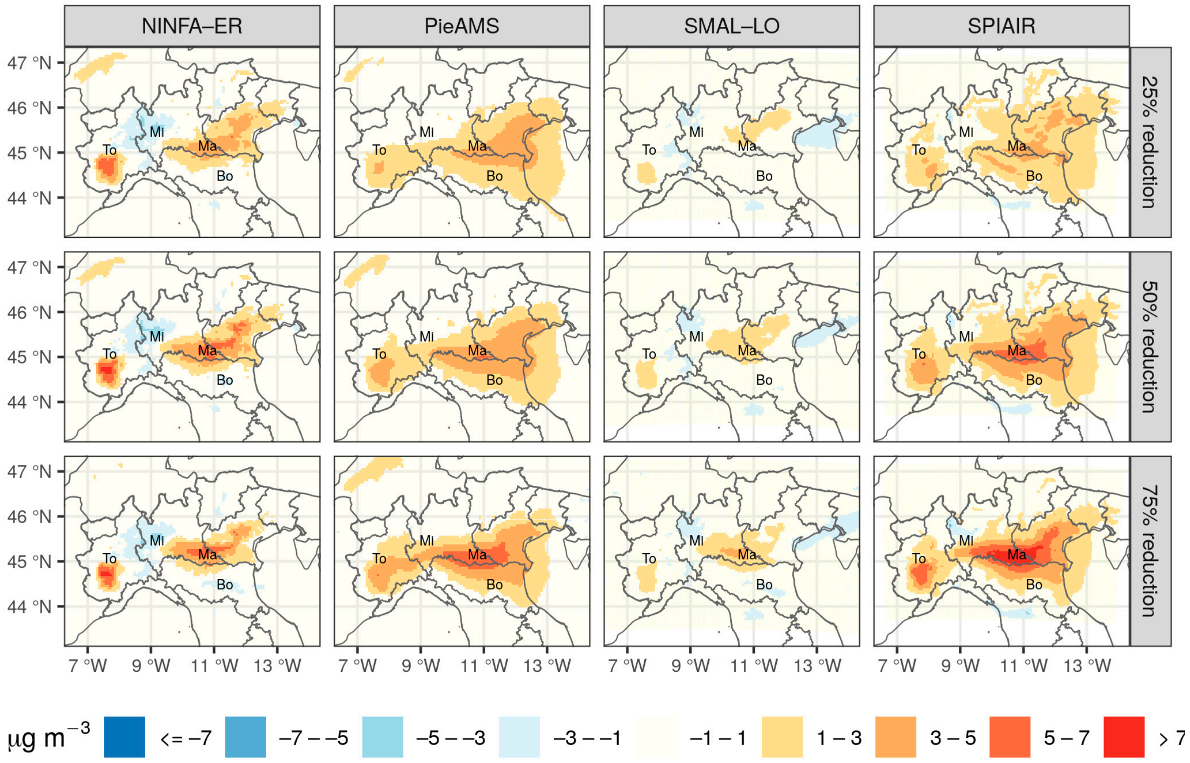

Figure 6. Simulated chemical regimes obtained for the cold season considering different levels of emission reductions: 25% (panels on top), 50% (panels in the centre) and 75% (panels at the bottom). The figure shows the difference $P^{\alpha}_{NOx} - P^{\alpha}_{NH3}$ with the unit µg m^{-3}. The abbreviations To, Mi, Ma and Bo indicate the location of Turin, Milan, Mantua and Bologna, respectively.

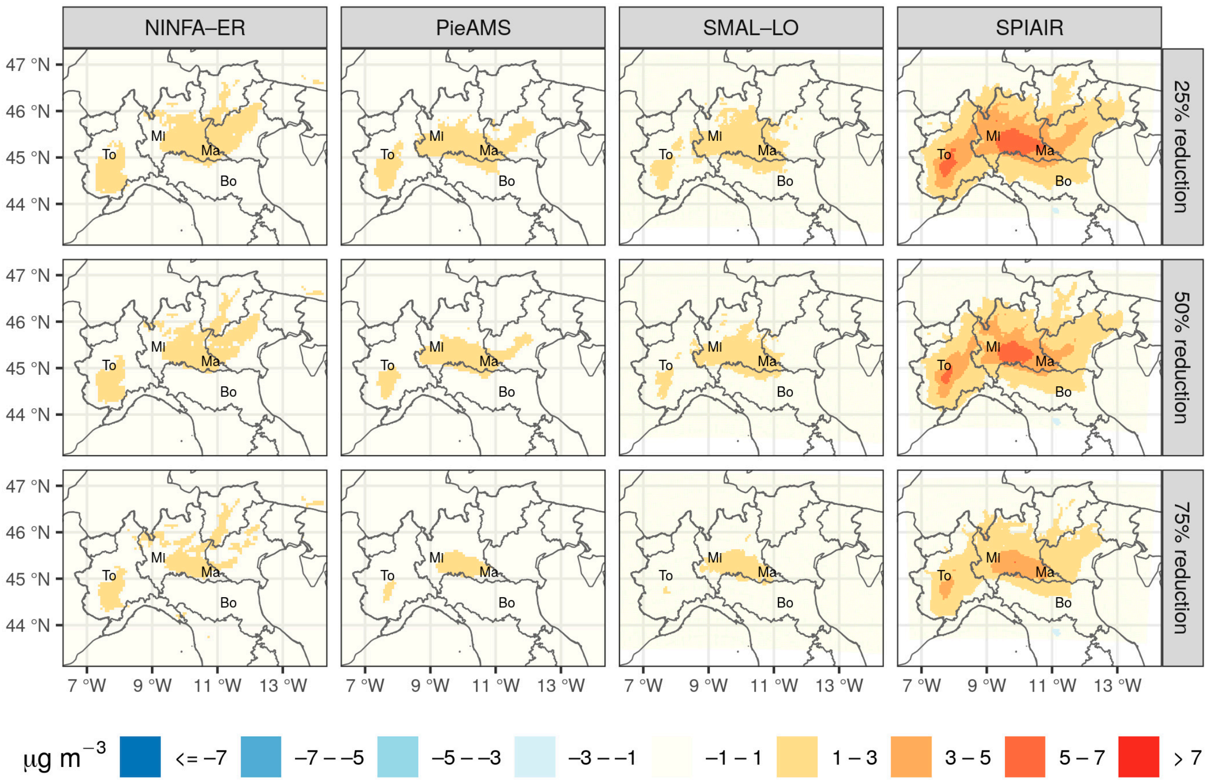

Figure 7. Same as Figure 6 but for the warm period.

During the cold season (Figure 6), the NO_x-sensitive regime tends to dominate a large part of the Po Valley, particularly in the area centred in Mantua (labelled as Ma in the maps) between Lombardy, Veneto and Emilia-Romagna. A second NO_x-sensitive spot is located in the province of Cuneo, around 50 km south of Turin (labelled as To) with different intensity depending on the modelling system. NH_3-sensitive zones are generally less pronounced with respect to NO_x-sensitive areas and located near Milan (labelled as Mi), between Lombardy and Piedmont regions and in Bologna, with the latter noticed only by SMAL-LO and NINFA-ER for strong emission reductions (75%).

Confirming the outcome of [31], NO_x-sensitive regimes correspond to those regions characterised by the highest agricultural emissions (NH_3) of the whole Po Valley [40], and NH_3-sensitive regimes are located in NO_x rich regions, such as the metropolitan area of Milan. In addition, the multi-model analysis highlights that non-linearities are characterised by a reinforcement of the respective chemical regimes (PIs are not constant with the emission reduction strength).

By comparing the results obtained in this study for 25% reduction with those of [31], three main findings can be observed. First, the extension and the absolute values of NH_3-sensitive areas found by [31] are larger and higher compared to those observed here. In [31], the NH_3-sensitive area encompasses the surrounding area of Milano, Bergamo, Crema and Manerbio up to Verona, in a triangular shape. Here, the NH_3-sensitive spot is mainly centred in Milan and does not extend to the east side of the Po Valley, but slightly scratches the west, as also highlighted by [31]. Secondly, the NO_x-sensitive areas found in this study roughly correspond to those of [31], for both location and magnitude. Finally, the main difference with respect to [31] is that by increasing the reduction strength, we did not observe a progressive shift in chemical regime, but rather a reinforcement of this latter. NO_x- and NH_3-sensitive areas remain in place and tend to increase in intensity moving from 25% to 75% reductions.

We believe that these discrepancies can be mainly attributed to a difference in the emission inventory and in the temporal modulation profile used to distribute the annual total. Indeed, the choice of the modulation profile for PM precursors seems to significantly affect model results in terms of both PI and chemical regimes, even if the total annual emission inventory is the same (see Figure 6, Figures S3 and S5).

Between April and September (warm period, see Figure 7), the entire Po Valley is characterised by weak NO_x-sensitive conditions, with a maximum intensity located in the central part of the domain, between Mantua and Milan (Lombardy region) and in the province of Cuneo (south of Turin, Piedmont), supporting the results obtained by [31] for the summer season. Unlike the cold period, by increasing the emission reductions, the chemical regime generally tends to reduce its extension and to decrease its intensity, making neutrality the prevailing regime in the Po Valley. However, for the SPIAIR system, the prevailing regime is NO_x-sensitive also with the strongest emission reduction considered in this study, although its extension progressively reduces with the reduction strength.

3.3. Analysis of Non-Linearities

As stated in the previous section, the Po Valley is dominated by significant variations in chemical regimes within a limited geographic area. These variations emphasise the role played by strong spatial emission gradients for both precursors. In areas with high NO_x emissions (such as the region near Milan), NH_3 becomes the limiting factor in secondary inorganic formation; conversely, the same role is played by NO_x in those regions with significant NH_3 emissions. In this section, additivity and consistency of PI are evaluated in both relative and absolute terms in order to quantify the effects of non-linearities.

Following Equation (2), when emission reductions are applied simultaneously to NO_x and NH_3, the reduction in $PM_{2.5}$ concentrations cannot be simply estimated as the sum of the reduction induced by single precursors; rather, an additional component, the interaction term, needs to be accounted for to assess the actual response of $PM_{2.5}$ concentrations. In Figure 8, information about the interaction term at the 25% reduction level is provided. The

PIs computed for the simultaneous reduction in NO_x and NH_3 (combined reduction) are plotted as a function of the sum of the single PI (sum reduction), and the deviation from the bisector quantifies the interaction term. For most of the points depicted in Figure 9, the interaction term is null or negative, and as indicated by the slope of the linear fit, it ranges between −11% and −6% for the warm period and is between −7% and −5% for both the cold period and the yearly average, confirming that for limited emission reductions (up to 25%), the non-linearity in Po Valley tends to be in the order of −10%, as also shown by other authors [88–91]. In other terms, the slope of the linear fit can be seen as a measure of how much the $PM_{2.5}$ concentrations would be overestimated if the individual NO_x and NH_3 reductions were linearly added.

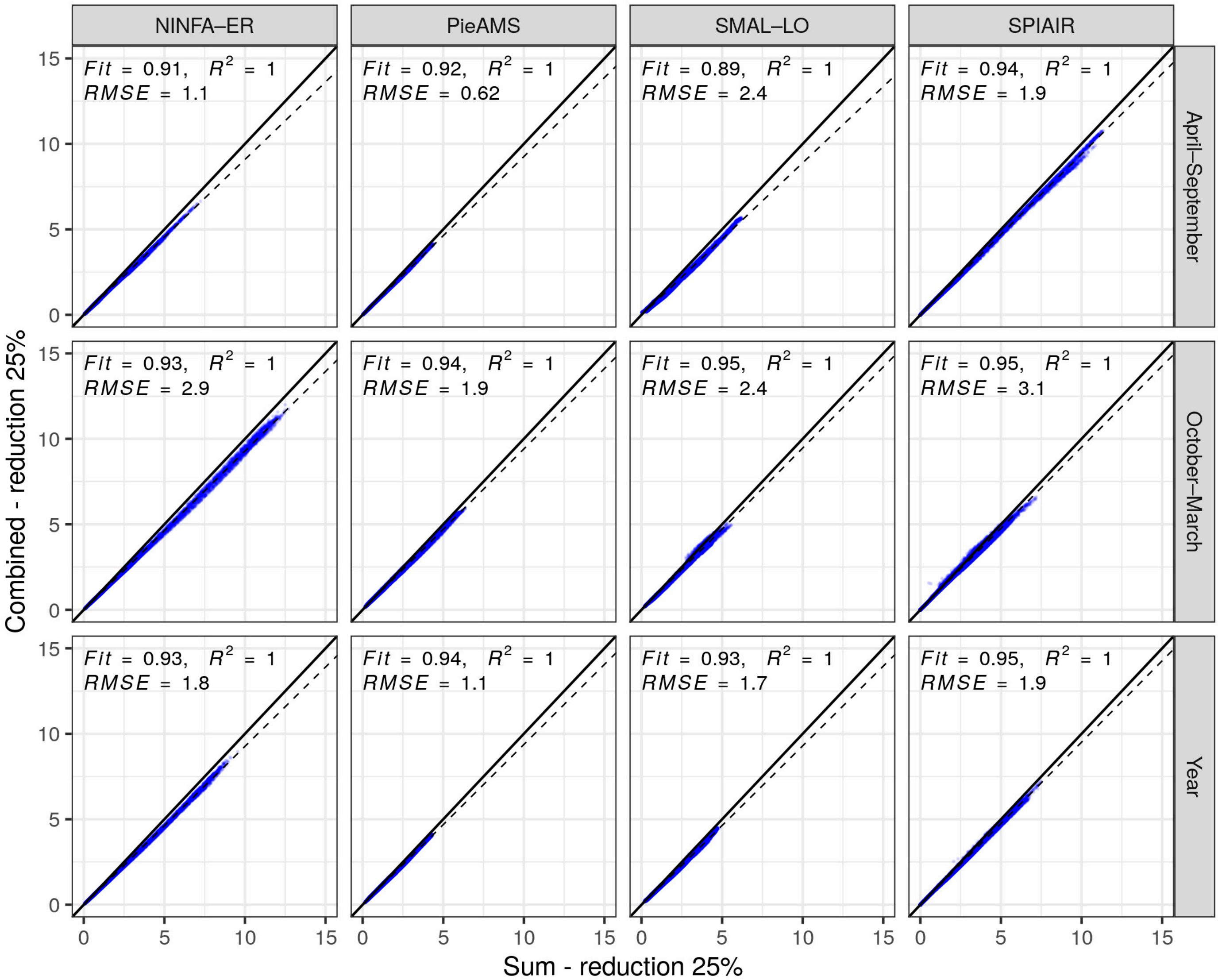

Figure 8. Non-linear interaction term for 25% emission reduction scenario. Comparison between the PI resulted from the simultaneous reduction in NO_x and NH_3 emissions (y-axis) and the sum of the PI computed from the single reduction in the two precursors (x-axis). Each point in the scatter plot represents a grid cell in the modelling domain, and the deviation from the bisector quantifies the interaction term of the total non-linearity. The axis units are μg m^{-3}.

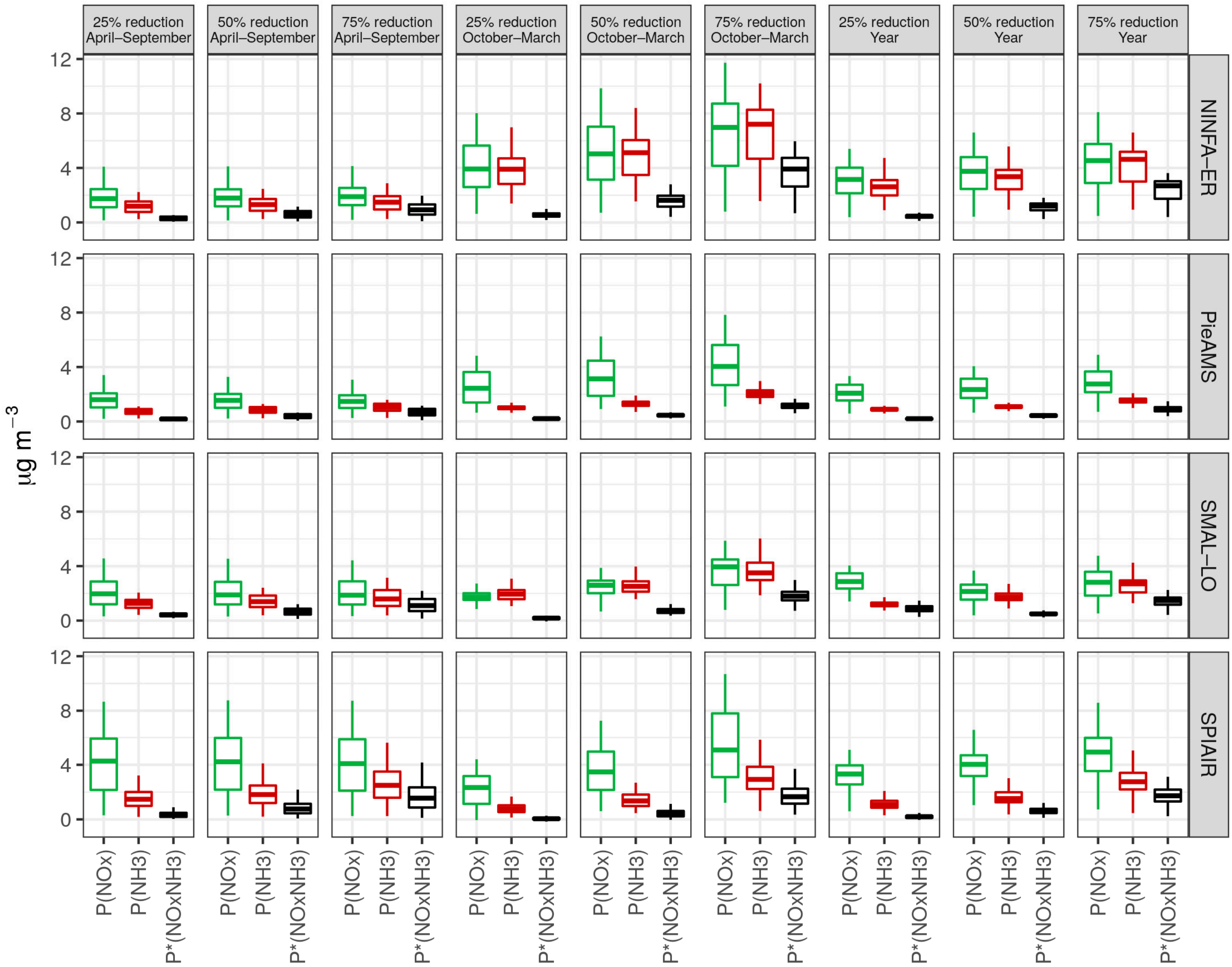

Figure 9. Boxplots of $PM_{2.5}$ potential impacts at station locations. $P(NO_x)$ and $P(NH_3)$ indicate potential impact computed from the reduction in NO_x and NH_3 emissions, respectively. $P^*(NO_xNH_3)$ is the difference between the sum of single potential impacts and the potential impact of the simultaneous reduction in both precursors. Results from NINFA-ER, SMAL-LO, PieAMS and SPIAIR are reported in the panels on the first, second, third and fourth row, respectively. The horizontal lines in a box indicate the median; the lower and upper ends of a box indicate the 25th and 75th percentiles, respectively.

The non-linear behaviour observed in Figure 8 can be explained by a shift in the chemical regime when reductions become more important, and the negative nature of this effect is due to the fact that a reduction in one of the two precursors involves a reduction in both the components (NO_3^- and NH_4^+) of ammonium nitrate. Therefore, the $PM_{2.5}$ reduction induced by jointly decreasing NO_x and NH_3 is lower than the effect caused by the sum of the two.

Figure 9 shows the PI of each reduction scenario simulated in this study, considering concentrations extracted at 85 station locations (see Figure 1). Boxplots coloured with green represent the PI of NO_x, those in red represent the PI of NH_3 and those in black represent the interaction term, of the opposite sign, of the simultaneous reduction in NO_x and NH_3 (Equation (3)). A distinction between warm and cold periods (labelled Apr–Sep and Oct–Mar, respectively), as well as for the yearly average (Year), is also made (see different columns). The results highlight that the PIs of both precursors tend to increase by increasing the reduction strength for yearly averages and for the winter period. This corresponds to an increase in efficiency toward higher percentages of emission reductions (i.e., an enhancement of positive non-linearity; see also further discussion in this section). In other terms, given that the relationship between the variation in $PM_{2.5}$ concentrations and the precursors' emission reductions is not constant within the range assessed (25–75%), PI cannot be used to interpolate or extrapolate the responses of other emission reduction levels.

On the other hand, during summertime, the response of the four modelling systems is generally more consistent than during wintertime, particularly for NO_x reductions, for which PIs remain almost constant in all the three reduction steps, showing limited non-linearities. In addition, during summer, the concentrations of ammonium and nitrate are on average very similar between models for all the simulated scenarios (Figure S4). The only exception is represented by SPIAIR, which generally tends to model higher nitrate concentrations compared to other models. These higher concentrations also seem to affect the efficiency in reducing the same nitrate, being generally higher for SPIAIR than the other models (Figure S6).

Focusing on the abatement of single precursors, the reduction in NO_x on average is more efficient than the reduction in NH_3, particularly during the warm period, when more than half of the total annual ammonia is emitted and $PM_{2.5}$ concentrations become more sensitive to NO_x emissions. Conversely, during winter, a contrasting behaviour is observed between the models. On average, NINFA-ER and SMAL-LO express similar PIs for NO_x and NH_3 reductions, while PieAMS and SPIAIR are clearly more sensitive to NO_x emissions. A possible explanation could be found in the differences in the reduction efficiency of ammonium and nitrate: these are higher for NINFA-ER and SMAL-LO compared to the other models during wintertime when NH_3 emissions are reduced (see SC3, SC6 and SC9 facets in Figure S5). Furthermore, as introduced in the previous section, we think that different temporal emission modulations can produce significant differences in the model behaviour during the same season. For example, looking at the PI of PieAMS and SMAL-LO during winter, even if they share the same CTM, the response to NH_3 reduction is considerably different. In fact, the efficiency in reducing nitrate for this season by SMAL-LO is on average higher than PieAMS (see SC3, SC6 and SC9 facets in Figure S5).

Valuable information on the additive property of linearity is provided in Figure 9. Black box plots highlight that when reductions do not overcome 25%, the interaction term tends to be limited below 1 $\mu g\ m^{-3}$ (about 10%, see Figure 8), while all the models agree with its increase toward higher percentages of emission reductions, on average up to 2–4 $\mu g\ m^{-3}$ (about 25–30% in relative terms, not shown), depending on the model considered.

Considering applying a certain reduction to both precursors (for example, 25% or 50%), and from that situation further increasing the reduction to a higher level (50% or 75%, respectively), three additional non-linear terms are generated (see the right side of Equation (4)) by comparing respective PIs. Each term represents a peculiar feature of the non-linearity. In particular, single precursor non-linearity (i.e., $\hat{P}^{\beta-\alpha}_{NOx}$ and $\hat{P}^{\beta-\alpha}_{NH3}$) tells us whether or not the chemical regime ($PM_{2.5}$ sensitivity to one precursor) is consistent with emission perturbations. High values of single precursor non-linearity indicate more variability in chemical regimes during emissions abatement, while low values lead to more stability. Conversely, the sum of the multi-precursor non-linear interaction terms ($\hat{P}^{\alpha}_{NOxNH3} + \hat{P}^{\beta-\alpha}_{NOxNH3}$) quantifies the strengthening (negative values) or the weakening (positive values) of the NO_x-NH_3 non-linear interaction term when stricter emission reductions are applied.

Figure 10 shows the PI variation when the reductions are increased from 25% to 50% and from 50% to 75% for the two periods considered in this study (April–September and October–March). Regardless of seasonality, it is worthwhile to note that all the modelling systems used in this study agree that reducing emissions increases the PI, which means that the overall non-linearities are positive and increase with the emission reduction strength. In relative terms, moving from 25% to 50% reduction, the non-linearity increases between 20% and 30% depending on the modelling system (see the linear fit slope) and between 10% and 40% from 50% to 75% reduction.

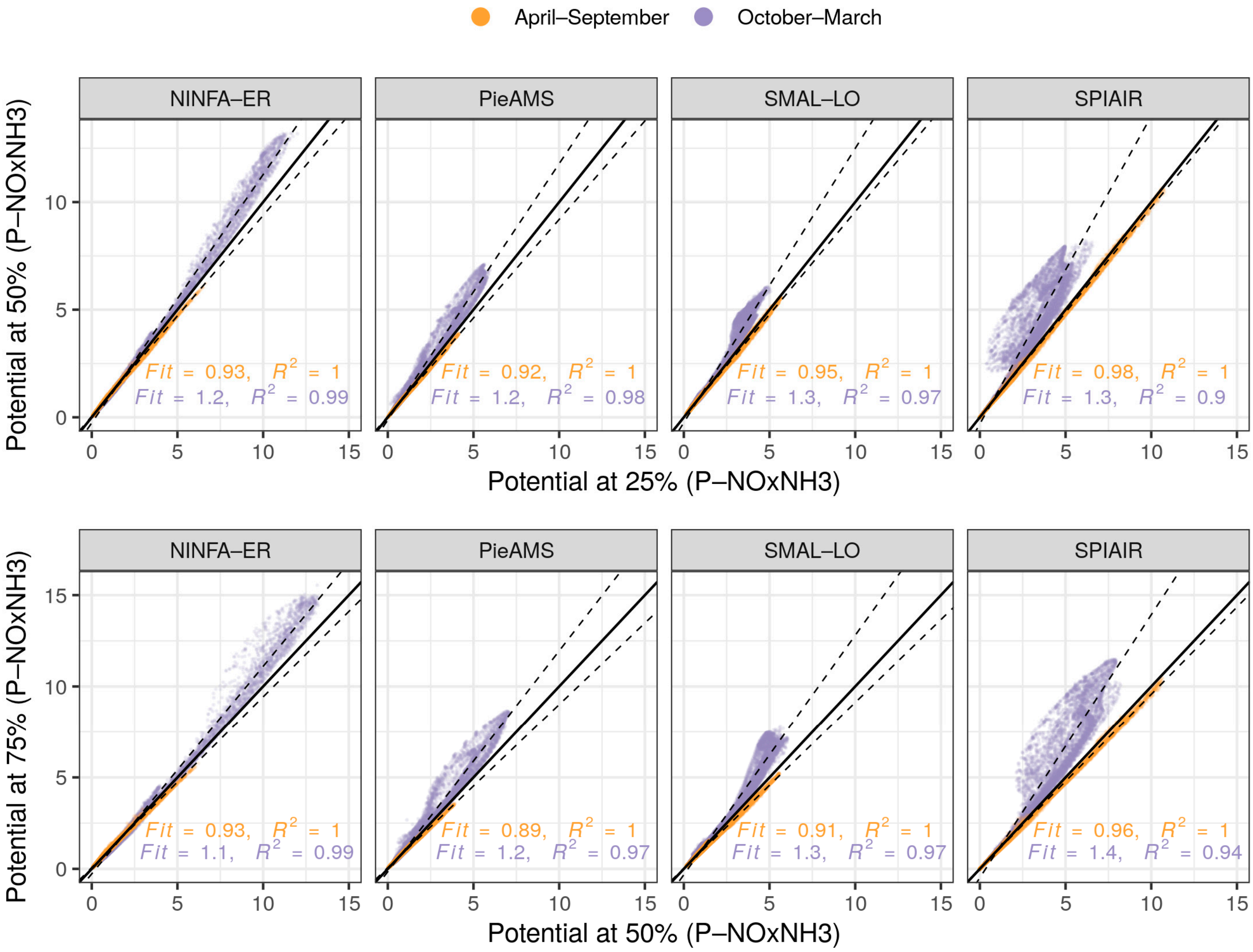

Figure 10. Scatter plots representing the relation between impacts of combined emission reduction in NO_x and NH_3 from 25% to 50% emission reduction (top panel) and from 50% to 75% (bottom panel). Dots represent a grid cell in the modelling domains, with blue for wintertime and yellow for summertime. The distance from the 1:1 line quantifies the magnitude of the overall non-linear terms.

On the other hand, during the warm period, PIs are slightly negative and decrease with the emission reduction strength, revealing a limited change in non-linearity when stricter emission reductions are applied for the warm period. More in detail, PI decreases between −2% and −7% (linear fit slope between 0.98 and 0.93) moving from 25% to 50% reduction and between −4% and −11% (linear fit slope between 0.96 and 0.89) moving from 50% to 75% reduction.

The relative increment in PIs seen in Figure 10 for the cold and warm periods can also be observed in absolute terms in Figures 11 and 12, where the total non-linearity introduced by increasing emission reduction is shown in terms of $\mu g\ m^{-3}$ through spatial maps. During the cold period (Figure 11), all modelling systems show an increment in non-linearities (green palettes) in the area centred in Mantua between Lombardy, Emilia-Romagna and Veneto for both reduction steps. The increment tends to be limited to 3 $\mu g\ m^{-3}$, with the only exception of SPIAIR, which shows generally higher values and a maximum increment of 3.8 $\mu g\ m^{-3}$ in the southern part of Lombardy when emissions are decreased from 50% to 75%. A possible explanation of this different behaviour can be found in the approach followed by SPIAIR for the vertical distribution of the anthropogenic emissions. In contrast to the other systems, all emissions are allocated to the first model layer, which may result in stronger effects on PI computation when high levels of reduction are applied.

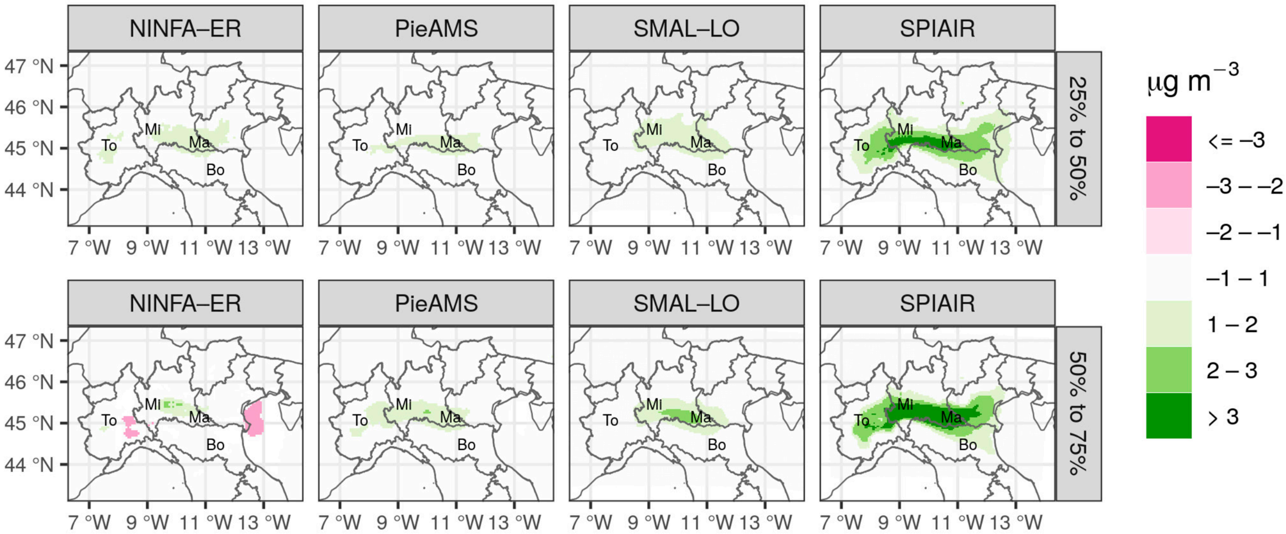

Figure 11. Wintertime (October–March) maps of the overall non-linearity term, expressed in absolute terms (μg m^{-3}).

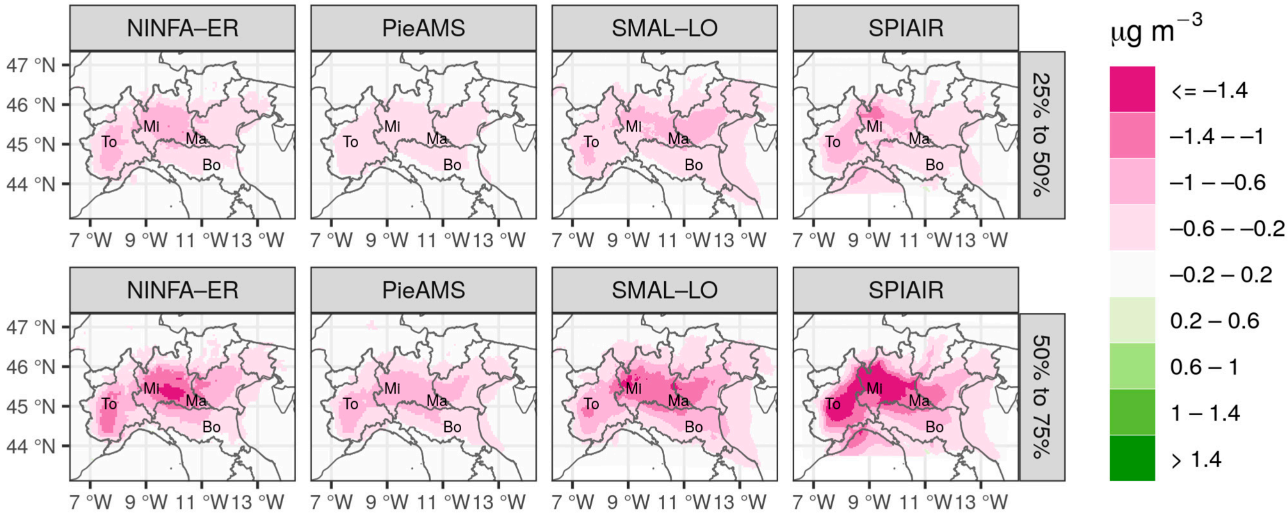

Figure 12. Summertime (April–September) maps of the overall non-linearity term, expressed in absolute terms (μg m^{-3}). It is important to note the different scale with respect to Figure 11.

Confirming the outcomes shown by other authors [31,32], by disentangling the total non-linearity in three terms (Equation (4) and Figure S7 in the Supplementary Materials), the total contribution is dominated by the single NO_x non-linearity (reinforcement of NO_x-sensitive regime), while the single NH_3 non-linearity has only a modest contribution. On the other hand, the non-linear interaction term tends to be neutral or slightly negative (violet palettes for negative values), indicating that the NO_x–NH_3 non-linearity increases upon moving from 25% to 50% and from 50% to 75% reductions (this latter case is not shown as spatial maps but is visible from the black box plot of Figure 9).

During the warm period (Figure 12), PI variations are smaller than those during the cold period (see different scale between Figures 11 and 12), and in contrast to this latter period, the overall non-linearities are slightly negative, which means that by increasing the reduction strength, the PI decreases. Figure S8 in the Supplementary Materials also shows that for the warm period, the multi-precursor non-linear interaction terms dominate the total non-linearity, implying a reinforcement of the $\hat{P}^{\alpha}_{NOxNH3}$ component, i.e., the more emissions are reduced, the more this latter term becomes negative, as observed for the cold period.

4. Discussion and Conclusions

When a decision maker has to decide whether to take a specific action for a specific air quality target, he/she needs to understand how this action affects different locations (i.e., spatial variability) and how much is efficient. Whereas it is quite simple to design successful solutions for non-reactive primary pollutants, it is much more complex for secondary compounds, for which the relation between emission reductions and concentrations abatement might not be linear.

This paper follows the scheme of recent works on $PM_{2.5}$ concentrations in the Po Valley [31,32], where a single CTM was used to simulate emission scenarios. In this study, four chemical transport models, used by four different Italian Environmental Agencies, were applied over the Po Valley to provide a robust response to reducing emissions of two important inorganic precursors, nitrogen oxides (NO_x) and ammonia (NH_3), in the formation of secondary $PM_{2.5}$. NO_x and NH_3 were reduced individually and simultaneously, from 25% to 75%, with the aim of providing insight about abatement strategies necessary to further reduce pollution levels.

To verify the robustness of the AQ modelling system responses, the base case was used to validate modelled $PM_{2.5}$, total ammonium and total nitrate concentrations with respect to observations at background stations. Modelled concentrations from emission reductions were also compared to the base case to describe the spatial and temporal variability of chemical regimes and to outline the reduction efficiency in terms of potential impacts (PI).

The first straightforward conclusion from our analysis is that for both summertime and wintertime, all the modelling systems simulate on average lower $PM_{2.5}$ concentrations when both precursors are jointly decreased. Besides this expected outcome, we found an important difference with respect to [31]. The four modelling systems did not observe an increase in $PM_{2.5}$ concentrations by reducing NO_x emissions. Even if the same explanation provided in [31] about the increase in the oxidative capacity of the atmosphere for limited NO_x reductions could hold here, the conditions experienced during this study did not bring an increase in ammonium and nitrate concentrations for the same reductions tested in [31]. Rather, we observed a progressive decrease (more than linear) in these two components toward stronger reductions, for both seasons. Different meteorological years (2019 here and 2015 in [31]) and different emission and model resolutions might have led to different outcomes. Indeed, the first reduction step at 25% may be too high to observe the same increase noted by [31] for the model set-ups and emission inventory used here. Thus, we think that additional tests at lower reduction steps (below 25%) are needed to provide more insight about the phenomenon observed by [31].

In the second part of the study, the analysis of PI and chemical regimes identified two contrasting chemical regimes during the cold season. NO_x-sensitive areas were detected in Mantua (between Lombardy, Veneto and Emilia-Romagna regions) and in the province of Cuneo (south of Turin), which correspond to NH_3 rich regions. On the other hand, a NH_3-sensitive spot is located near Milan and between Lombardy and Piedmont, where NO_x emissions are generally high. It is interesting that, by comparing the results of this paper with those obtained in [31] for winter, the extension of the NH_3-sensitive area observed here encompasses only the territory surrounding Milan, whereas in [31], the NH_3-sensitive area covers a large part of the Northern Po Valley, from Milan to Verona. The same area in [31] was also under strong NH_3-sensitive conditions, while here, NH_3-sensitive spots were generally weak. Moreover, [31] noted a progressive shift in chemical regime toward stronger reductions, which was not found here for any of the modelling systems. Conversely, we observed a reinforcement of both the chemical regimes when moving from low to higher emission reductions. A possible explanation could be found in the differences in the emission inventories and in the temporal modulation profiles used to allocate emissions during the year. In addition, the usage of different meteorological years can also produce significant differences in model responses in the identification of chemical regimes.

During summertime, the situation changes: although the neutrality of PI between NO_x and NH_3 tends to predominate, particularly for strong emission reductions, $PM_{2.5}$ concentrations are characterised by weak NO_x-sensitive conditions, with the highest intensity occurring between Mantua and Milan, confirming more similarities between this study and [31] in summer.

Although the assessment of chemical regimes may imply counter-intuitive actions, a reduction in NO_x emissions over NO_x-sensitive areas and a reduction in NH_3 emissions over NH_3-sensitive areas would be the most efficient abatement strategy for decreasing $PM_{2.5}$ concentrations.

The analysis of non-linearities revealed that during the cold season, the PIs tend to increase by increasing the emission reductions, particularly in those areas identified as NO_x-sensitive, expressing positive non-linearities for each reduction considered (i.e., the more emissions are reduced, the more efficiently $PM_{2.5}$ concentrations are decreased, as similarly concluded by [31]). During summertime, the magnitude of non-linearities is smaller than in wintertime and PIs tend to remain almost constant, or slightly negative, by increasing the emission reductions. Since wintertime $PM_{2.5}$ concentrations are higher than in summertime, it is possible to conclude that strong emission reductions should be envisaged to maximise reduction effectiveness.

This study also found that by increasing the reduction strength, the difference between the PI of the simultaneous reduction in NO_x and NH_3 and the sum of a single PI increases for both seasons, being limited to 1 $\mu g\ m^{-3}$ (10% in relative terms and thus manageable in terms of air quality planning) for limited emission reductions (25%) and increasing on average up to 4 $\mu g\ m^{-3}$ (about 30%) for 75% emission reductions, which cannot be neglected in the design of air quality plans.

To conclude, to carefully determine whether further $PM_{2.5}$ abatement may be achieved, additional simulations aimed at exploring the effects of other precursor reductions should be performed. Other key pollutants in the formation of secondary $PM_{2.5}$ are sulphur dioxide (SO_2) and non-methane volatile organic compounds. Although SO_2 has generally low concentrations in the Po Valley, its further reduction may lead to additional $PM_{2.5}$ decreases, as stated in [32], because of its involvement in secondary particulate processes. Non-methane volatile organic compounds could also have an important impact since they affect oxidant concentrations and, consequently, nitrate and sulphate formation.

Supplementary Materials: The following supporting information can be downloaded at: https://www.mdpi.com/article/10.3390/atmos14050762/s1, Section S1: Models evaluation [86,87]; Figure S1: Model Quality Indicator (MQI) computed for yearly average $PM_{2.5}$ model results; Figure S2: Comparison between modelled and observed total ammonium and total nitrate with related confidence interval at 95% level for wintertime, summertime and yearly average; Figure S3: Winter-averaged concentrations of total ammonium and total nitrate extracted at super-site locations for each simulated scenario; Figure S4: Summer-averaged concentrations of total ammonium and total nitrate extracted at super-site locations for each simulated scenario; Figure S5: Winter-averaged PI of total ammonium and nitrate extracted at super-site locations for each simulated scenario; S6: Summer-averaged PI of total ammonium and nitrate extracted at super-site locations for each simulated scenario; Figure S7: Wintertime maps of the components of the total non-linearity, expressed as PI ($\mu g\ m^{-3}$) between 25% and 50% emission reduction; Figure S8: Summertime maps of the components of the total non-linearity, expressed as PI ($\mu g\ m^{-3}$) between 25% and 50% emission reduction.

Author Contributions: Conceptualisation, M.S., S.B., E.A., L.C., A.D.F. and G.V.; methodology, G.V., L.C., S.B., M.S., A.M.; software, G.V., M.S., S.B., L.C., A.M., A.D.F., B.I., F.B. and S.G.; formal analysis, G.V., L.C., S.B. and A.D.F.; investigation, G.V., L.C., S.B., A.D.F. and S.P.; resources, M.S., S.B. and E.A.; data curation, G.V., L.C., A.D.F., B.I., G.F., G.M., A.M., S.G., F.B., L.B., R.A. and G.G.; writing—original draft preparation, G.V.; writing—review and editing, L.C., L.B., S.B., A.M., E.A. and A.D.F.; supervision, M.S., E.A., S.B. and A.D.F. All authors have read and agreed to the published version of the manuscript.

Funding: This research was funded by the LIFE-IP PREPAIR (Po Regions Engaged to Policies of AIR) project, Grant Number LIFE15 IPE/IT/000013.

Institutional Review Board Statement: Not applicable.

Informed Consent Statement: Not applicable.

Data Availability Statement: Not applicable.

Acknowledgments: Acknowledgments are given to all the beneficiaries of the project LIFE-IP PREPAIR: Emilia-Romagna Region (Project Coordinator) Veneto Region, Lombardy Region, Piedmont Region, Friuli Venezia Giulia Region, Autonomous Province of Trento, Regional Agency for Environment of Emilia-Romagna (ARPAE), Regional Agency for Environment of Veneto, Regional Agency for Environment of Piedmont, Regional Agency for Environmental Protection of Lombardy, Environmental Protection Agency of Valle d'Aosta, Environmental Protection Agency of Friuli Venezia Giulia, Slovenian Environment Agency, Municipality of Bologna, Municipality of Milan, City of Turin, ART-ER, Lombardy Foundation for Environment.

Conflicts of Interest: The authors declare no conflict of interest.

References

1. Kim, K.-H.; Kabir, E.; Kabir, S. A Review on the Human Health Impact of Airborne Particulate Matter. *Environ. Int.* **2015**, *74*, 136–143. [CrossRef]
2. Anderson, J.O.; Thundiyil, J.G.; Stolbach, A. Clearing the Air: A Review of the Effects of Particulate Matter Air Pollution on Human Health. *J. Med. Toxicol.* **2012**, *8*, 166–175. [CrossRef] [PubMed]
3. Alemayehu, Y.A.; Asfaw, S.L.; Terfie, T.A. Exposure to Urban Particulate Matter and Its Association with Human Health Risks. *Environ. Sci. Pollut. Res.* **2020**, *27*, 27491–27506. [CrossRef] [PubMed]
4. Loomis, D.; Grosse, Y.; Lauby-Secretan, B.; El Ghissassi, F.; Bouvard, V.; Benbrahim-Tallaa, L.; Guha, N.; Baan, R.; Mattock, H.; Straif, K.; et al. The Carcinogenicity of Outdoor Air Pollution. *Lancet Oncol.* **2013**, *14*, 1262–1263. [CrossRef]
5. West, J.J.; Cohen, A.; Dentener, F.; Brunekreef, B.; Zhu, T.; Armstrong, B.; Bell, M.L.; Brauer, M.; Carmichael, G.; Costa, D.L.; et al. What We Breathe Impacts Our Health: Improving Understanding of the Link between Air Pollution and Health. *Environ. Sci. Technol.* **2016**, *50*, 4895–4904. [CrossRef] [PubMed]
6. Du, Y.; Xu, X.; Chu, M.; Guo, Y.; Wang, J. Air Particulate Matter and Cardiovascular Disease: The Epidemiological, Biomedical and Clinical Evidence. *J. Thorac. Dis.* **2016**, *8*, E8–E19. [CrossRef]
7. Fiordelisi, A.; Piscitelli, P.; Trimarco, B.; Coscioni, E.; Iaccarino, G.; Sorriento, D. The Mechanisms of Air Pollution and Particulate Matter in Cardiovascular Diseases. *Heart Fail. Rev.* **2017**, *22*, 337–347. [CrossRef]
8. Kim, H.; Kim, W.-H.; Kim, Y.-Y.; Park, H.-Y. Air Pollution and Central Nervous System Disease: A Review of the Impact of Fine Particulate Matter on Neurological Disorders. *Front. Public Health* **2020**, *8*, 575330. [CrossRef]
9. Hamra, G.B.; Guha, N.; Cohen, A.; Laden, F.; Raaschou-Nielsen, O.; Samet, J.M.; Vineis, P.; Forastiere, F.; Saldiva, P.; Yorifuji, T.; et al. Outdoor Particulate Matter Exposure and Lung Cancer: A Systematic Review and Meta-Analysis. *Environ. Health Perspect.* **2014**, *122*, 906–911. [CrossRef]
10. Wei, Y.; Wang, Y.; Di, Q.; Choirat, C.; Wang, Y.; Koutrakis, P.; Zanobetti, A.; Dominici, F.; Schwartz, J.D. Short Term Exposure to Fine Particulate Matter and Hospital Admission Risks and Costs in the Medicare Population: Time Stratified, Case Crossover Study. *BMJ* **2019**, *367*, l6258. [CrossRef]
11. Pearson, J.F.; Bachireddy, C.; Shyamprasad, S.; Goldfine, A.B.; Brownstein, J.S. Association Between Fine Particulate Matter and Diabetes Prevalence in the U.S. *Diabetes Care* **2010**, *33*, 2196–2201. [CrossRef]
12. Chen, H.; Burnett, R.T.; Kwong, J.C.; Villeneuve, P.; Goldberg, M.S.; Brook, R.D.; Van Donkelaar, A.; Jerrett, M.; Martin, R.; Brook, J.R.; et al. Risk of Incident Diabetes in Relation to Long-Term Exposure to Fine Particulate Matter in Ontario, Canada. *Environ. Health Perspect.* **2013**, *121*, 804–810. [CrossRef]
13. O'Piela, D.R.; Durisek, G.R.; Escobar, Y.-N.H.; Mackos, A.R.; Wold, L.E. Particulate Matter and Alzheimer's Disease: An Intimate Connection. *Trends Mol. Med.* **2022**, *28*, 770–780. [CrossRef]
14. WHO Global Air Quality Guidelines: Particulate Matter (PM2.5 and PM10), Ozone, Nitrogen Dioxide, Sulfur Dioxide and Carbon Monoxide. Available online: https://www.who.int/publications-detail-redirect/9789240034228 (accessed on 24 January 2023).
15. European R Commission. *Directive 2008/50/EC of the European Parliament and of the Council of 21 May 2008 on Ambient Air Quality and Cleaner Air for Europe*; European Commission: Brussels, Belgium, 2008; Volume 152.
16. Raffaelli, K.; Deserti, M.; Stortini, M.; Amorati, R.; Vasconi, M.; Giovannini, G. Improving Air Quality in the Po Valley, Italy: Some Results by the LIFE-IP-PREPAIR Project. *Atmosphere* **2020**, *11*, 429. [CrossRef]
17. Bigi, A.; Ghermandi, G. Trends and Variability of Atmospheric $PM_{2.5}$ and $PM_{10-2.5}$ Concentration in the Po Valley, Italy. *Atmos. Chem. Phys.* **2016**, *16*, 15777–15788. [CrossRef]

18. Bigi, A.; Bianchi, F.; De Gennaro, G.; Di Gilio, A.; Fermo, P.; Ghermandi, G.; Prévôt, A.S.H.; Urbani, M.; Valli, G.; Vecchi, R.; et al. Hourly Composition of Gas and Particle Phase Pollutants at a Central Urban Background Site in Milan, Italy. *Atmos. Res.* **2017**, *186*, 83–94. [CrossRef]
19. Meroni, A.; Pirovano, G.; Gilardoni, S.; Lonati, G.; Colombi, C.; Gianelle, V.; Paglione, M.; Poluzzi, V.; Riva, G.M.; Toppetti, A. Investigating the Role of Chemical and Physical Processes on Organic Aerosol Modelling with CAMx in the Po Valley during a Winter Episode. *Atmos. Environ.* **2017**, *171*, 126–142. [CrossRef]
20. Tositti, L.; Brattich, E.; Masiol, M.; Baldacci, D.; Ceccato, D.; Parmeggiani, S.; Stracquadanio, M.; Zappoli, S. Source Apportionment of Particulate Matter in a Large City of Southeastern Po Valley (Bologna, Italy). *Environ. Sci. Pollut. Res.* **2014**, *21*, 872–890. [CrossRef] [PubMed]
21. Canepari, S.; Astolfi, M.L.; Farao, C.; Maretto, M.; Frasca, D.; Marcoccia, M.; Perrino, C. Seasonal Variations in the Chemical Composition of Particulate Matter: A Case Study in the Po Valley. Part II: Concentration and Solubility of Micro- and Trace-Elements. *Environ. Sci. Pollut. Res. Int.* **2014**, *21*, 4010–4022. [CrossRef]
22. Perrino, C.; Catrambone, M.; Dalla Torre, S.; Rantica, E.; Sargolini, T.; Canepari, S. Seasonal Variations in the Chemical Composition of Particulate Matter: A Case Study in the Po Valley. Part I: Macro-Components and Mass Closure. *Environ. Sci. Pollut. Res.* **2014**, *21*, 3999–4009. [CrossRef]
23. Błaszczak, B.; Zioła, N.; Mathews, B.; Klejnowski, K.; Słaby, K. The Role of PM2.5 Chemical Composition and Meteorology during High Pollution Periods at a Suburban Background Station in Southern Poland. *Aerosol Air Qual. Res.* **2020**, *20*, 2433–2447. [CrossRef]
24. Vieno, M.; Heal, M.R.; Twigg, M.M.; MacKenzie, I.A.; Braban, C.F.; Lingard, J.J.N.; Ritchie, S.; Beck, R.C.; Móring, A.; Ots, R.; et al. The UK Particulate Matter Air Pollution Episode of March–April 2014: More than Saharan Dust. *Environ. Res. Lett.* **2016**, *11*, 044004. [CrossRef]
25. Harrison, R.M.; Beddows, D.C.S.; Tong, C.; Damayanti, S. Non-Linearity of Secondary Pollutant Formation Estimated from Emissions Data and Measured Precursor-Secondary Pollutant Relationships. *Npj Clim. Atmos. Sci.* **2022**, *5*, 71. [CrossRef]
26. Beekmann, M.; Prévôt, A.S.H.; Drewnick, F.; Sciare, J.; Pandis, S.N.; Denier van der Gon, H.a.C.; Crippa, M.; Freutel, F.; Poulain, L.; Ghersi, V.; et al. In Situ, Satellite Measurement and Model Evidence on the Dominant Regional Contribution to Fine Particulate Matter Levels in the Paris Megacity. *Atmos. Chem. Phys.* **2015**, *15*, 9577–9591. [CrossRef]
27. Petit, J.-E.; Amodeo, T.; Meleux, F.; Bessagnet, B.; Menut, L.; Grenier, D.; Pellan, Y.; Ockler, A.; Rocq, B.; Gros, V.; et al. Characterising an Intense PM Pollution Episode in March 2015 in France from Multi-Site Approach and near Real Time Data: Climatology, Variabilities, Geographical Origins and Model Evaluation. *Atmos. Environ.* **2017**, *155*, 68–84. [CrossRef]
28. Wang, Q.; Li, S. Nonlinear Impact of COVID-19 on Pollutions—Evidence from Wuhan, New York, Milan, Madrid, Bandra, London, Tokyo and Mexico City. *Sustain. Cities Soc.* **2021**, *65*, 102629. [CrossRef]
29. Ciarelli, G.; Jiang, J.; Haddad, I.E.; Bigi, A.; Aksoyoglu, S.; Prévôt, A.S.H.; Marinoni, A.; Shen, J.; Yan, C.; Bianchi, F. Modeling the Effect of Reduced Traffic Due to COVID-19 Measures on Air Quality Using a Chemical Transport Model: Impacts on the Po Valley and the Swiss Plateau Regions. *Environ. Sci. Atmos.* **2021**, *1*, 228–240. [CrossRef] [PubMed]
30. Clappier, A.; Pisoni, E.; Thunis, P. A New Approach to Design Source–Receptor Relationships for Air Quality Modelling. *Environ. Model. Softw.* **2015**, *74*, 66–74. [CrossRef]
31. Thunis, P.; Clappier, A.; Beekmann, M.; Putaud, J.P.; Cuvelier, C.; Madrazo, J.; de Meij, A. Non-Linear Response of $PM_{2.5}$ to Changes in NO_x and NH_3 Emissions in the Po Basin (Italy): Consequences for Air Quality Plans. *Atmos. Chem. Phys.* **2021**, *21*, 9309–9327. [CrossRef]
32. Clappier, A.; Thunis, P.; Beekmann, M.; Putaud, J.P.; de Meij, A. Impact of SOx, NOx and NH3 Emission Reductions on PM2.5 Concentrations across Europe: Hints for Future Measure Development. *Environ. Int.* **2021**, *156*, 106699. [CrossRef]
33. Mailler, S.; Menut, L.; Khvorostyanov, D.; Valari, M.; Couvidat, F.; Siour, G.; Turquety, S.; Briant, R.; Tuccella, P.; Bessagnet, B.; et al. CHIMERE-2017: From Urban to Hemispheric Chemistry-Transport Modeling. *Geosci. Model Dev.* **2017**, *10*, 2397–2423. [CrossRef]
34. Menut, L.; Bessagnet, B.; Briant, R.; Cholakian, A.; Couvidat, F.; Mailler, S.; Pennel, R.; Siour, G.; Tuccella, P.; Turquety, S.; et al. The CHIMERE V2020r1 Online Chemistry-Transport Model. *Geosci. Model Dev.* **2021**, *14*, 6781–6811. [CrossRef]
35. Gariazzo, C.; Silibello, C.; Finardi, S.; Radice, P.; Piersanti, A.; Calori, G.; Cecinato, A.; Perrino, C.; Nussio, F.; Cagnoli, M.; et al. A Gas/Aerosol Air Pollutants Study over the Urban Area of Rome Using a Comprehensive Chemical Transport Model. *Atmos. Environ.* **2007**, *41*, 7286–7303. [CrossRef]
36. Silibello, C.; Calori, G.; Brusasca, G.; Giudici, A.; Angelino, E.; Fossati, G.; Peroni, E.; Buganza, E. Modelling of PM10 Concentrations over Milano Urban Area Using Two Aerosol Modules. *Environ. Model. Softw.* **2008**, *23*, 333–343. [CrossRef]
37. Dalla-Fontana, A.; Pillon, S.; Patti, S. A Performance Evaluation of the CAMx Air Quality Model to Forecast Ozone and PM_{10} over the Italian Region of Veneto. *Tethys J. Weather Clim. West. Mediterrania* **2021**, *18*, 1–13. [CrossRef]
38. Ciarelli, G.; Aksoyoglu, S.; Crippa, M.; Jimenez, J.-L.; Nemitz, E.; Sellegri, K.; Äijälä, M.; Carbone, S.; Mohr, C.; O'Dowd, C.; et al. Evaluation of European Air Quality Modelled by CAMx Including the Volatility Basis Set Scheme. *Atmos. Chem. Phys.* **2016**, *16*, 10313–10332. [CrossRef]
39. Nopmongcol, U.; Koo, B.; Tai, E.; Jung, J.; Piyachaturawat, P.; Emery, C.; Yarwood, G.; Pirovano, G.; Mitsakou, C.; Kallos, G. Modeling Europe with CAMx for the Air Quality Model Evaluation International Initiative (AQMEII). *Atmos. Environ.* **2012**, *53*, 177–185. [CrossRef]

40. Marongiu, A.; Angelino, E.; Moretti, M.; Malvestiti, G.; Fossati, G. Atmospheric Emission Sources in the Po-Basin from the LIFE-IP PREPAIR Project. *Open J. Air Pollut.* **2022**, *11*, 70–83. [CrossRef]
41. Stortini, M.; Arvani, B.; Deserti, M. Operational Forecast and Daily Assessment of the Air Quality in Italy: A Copernicus-CAMS Downstream Service. *Atmosphere* **2020**, *11*, 447. [CrossRef]
42. Derognat, C.; Beekmann, M.; Baeumle, M.; Martin, D.; Schmidt, H. Effect of Biogenic Volatile Organic Compound Emissions on Tropospheric Chemistry during the Atmospheric Pollution Over the Paris Area (ESQUIF) Campaign in the Ile-de-France Region. *J. Geophys. Res. Atmos.* **2003**, *108*, D17. [CrossRef]
43. Carter, W.P.L. Documentation of the Saprc-99 Chemical Mechanism for Voc Reactivity Assessment Volume 1 of 2 Documentation Text. Available online: https://intra.engr.ucr.edu/~carter/pubs/s99doc.pdf (accessed on 2 March 2023).
44. Yarwood, G.; Rao, S.; Way, R.; Yocke, M.; Whitten, G.Z.; Reyes, S. Luecken, Updates to the carbon bond chemical mechanism: CB05. D. U.S. Environmental Protection Agency Research Triangle Park: NC, USA, 2005. Available online: https://camx-wp.azurewebsites.net/Files/CB05_Final_Report_120805.pdf (accessed on 3 March 2023).
45. Simpson, D. Long-Period Modelling of Photochemical Oxidants in Europe. Model Calculations for July 1985. *Atmos. Environ. Part Gen. Top.* **1992**, *26*, 1609–1634. [CrossRef]
46. DeMore, W.B.; Sander, S.P.; Howard, C.J.; Ravishankara, A.R. Chemical Kinetics and Photochemical Data for Use in Stratospheric Modeling. Available online: https://jpldataeval.jpl.nasa.gov/pdf/Atmos97_Anotated.pdf (accessed on 4 March 2023).
47. Atkinson, R.; Baulch, D.L.; Cox, R.A.; Hampson, R.F.; Kerr, J.A.; Rossi, M.J.; Troe, J. Evaluated Kinetic, Photochemical and Heterogeneous Data for Atmospheric Chemistry: Supplement V. IUPAC Subcommittee on Gas Kinetic Data Evaluation for Atmospheric Chemistry. *J. Phys. Chem. Ref. Data* **1997**, *26*, 521–1011. [CrossRef]
48. Binkowski, F.S.; Roselle, S.J. Models-3 Community Multiscale Air Quality (CMAQ) Model Aerosol Component 1. Model Description. *J. Geophys. Res. Atmospheres* **2003**, *108*, D6. [CrossRef]
49. Emep_Report_1_Part1_2003.pdf. Available online: https://www.emep.int/publ/reports/2003/emep_report_1_part1_2003.pdf (accessed on 24 January 2023).
50. Whitby, K.T. The Physical Characteristics of Sulfur Aerosols. *Atmos. Environ.* **1978**, *12*, 135–159. [CrossRef]
51. Marsigli, C.; Boccanera, F.; Montani, A.; Paccagnella, T. The COSMO-LEPS Mesoscale Ensemble System: Validation of the Methodology and Verification. *Nonlinear Process. Geophys.* **2005**, *12*, 527–536. [CrossRef]
52. Gastaldo, T.; Poli, V.; Marsigli, C.; Cesari, D.; Alberoni, P.P.; Paccagnella, T. Assimilation of Radar Reflectivity Volumes in a Pre-Operational Framework. *Q. J. R. Meteorol. Soc.* **2021**, *147*, 1031–1054. [CrossRef]
53. Skamarock, C.; Klemp, B.; Dudhia, J.; Gill, O.; Barker, D.; Duda, G.; Huang, X.; Wang, W.; Powers, G. *A Description of the Advanced Research WRF Version 3*; University Corporation for Atmospheric Research: Boulder, CO, USA, 2008. [CrossRef]
54. Pernigotti, D.; Georgieva, E.; Thunis, P.; Bessagnet, B. Impact of Meteorology on Air Quality Modeling over the Po Valley in Northern Italy. *Atmos. Environ.* **2012**, *51*, 303–310. [CrossRef]
55. Kong, X.; Forkel, R.; Sokhi, R.S.; Suppan, P.; Baklanov, A.; Gauss, M.; Brunner, D.; Barò, R.; Balzarini, A.; Chemel, C.; et al. Analysis of Meteorology–Chemistry Interactions during Air Pollution Episodes Using Online Coupled Models within AQMEII Phase-2. *Atmos. Environ.* **2015**, *115*, 527–540. [CrossRef]
56. Brunner, D.; Savage, N.; Jorba, O.; Eder, B.; Giordano, L.; Badia, A.; Balzarini, A.; Baró, R.; Bianconi, R.; Chemel, C.; et al. Comparative Analysis of Meteorological Performance of Coupled Chemistry-Meteorology Models in the Context of AQMEII Phase 2. *Atmos. Environ.* **2015**, *115*, 470–498. [CrossRef]
57. Im, U.; Bianconi, R.; Solazzo, E.; Kioutsioukis, I.; Badia, A.; Balzarini, A.; Baró, R.; Bellasio, R.; Brunner, D.; Chemel, C.; et al. Evaluation of Operational Online-Coupled Regional Air Quality Models over Europe and North America in the Context of AQMEII Phase 2. Part II: Particulate Matter. *Atmos. Environ.* **2015**, *115*, 421–441. [CrossRef]
58. Troen, I.B.; Mahrt, L. A Simple Model of the Atmospheric Boundary Layer; Sensitivity to Surface Evaporation. *Bound.-Layer Meteorol.* **1986**, *37*, 129–148. [CrossRef]
59. Van Leer, B. Towards the Ultimate Conservative Difference Scheme. IV. A New Approach to Numerical Convection. *J. Comput. Phys.* **1977**, *23*, 276–299. [CrossRef]
60. Lange, R. Transferability of a Three-Dimensional Air Quality Model between Two Different Sites in Complex Terrain. *J. Appl. Meteorol. Climatol.* **1989**, *28*, 665–679. [CrossRef]
61. Nasstrom, J.S. *Turbulence Parameterizations for the Random Displacement Method (RDM) Version of ADPIC*; Lawrence Livermore National Lab. (LLNL): Livermore, CA, USA; EG and G Energy Measurements, Inc.: Las Vegas, NV, USA, 1995.
62. Smagorinsky, J. General Circulation Experiments with the Primitive Equations: I. The Basic Experiment. *Mon. Weather Rev.* **1963**, *91*, 99–164. [CrossRef]
63. Yamartino, R.J. Nonnegative, Conserved Scalar Transport Using Grid-Cell-Centered, Spectrally Constrained Blackman Cubics for Applications on a Variable-Thickness Mesh. *Mon. Weather Rev.* **1993**, *121*, 753–763. [CrossRef]
64. Yamartino, R.J.; Scire, J.S.; Carmichael, G.R.; Chang, Y.S. The CALGRID Mesoscale Photochemical Grid Model—I. Model Formulation. *Atmos. Environ. Part Gen. Top.* **1992**, *26*, 1493–1512. [CrossRef]

65. LeDuc, S.; Fine, S. Models-3/Community multiscale air quality (CMAQ) modeling system. In *Air Pollution Modeling and Its Application XV*; Borrego, C., Schayes, G., Eds.; Springer US: Boston, MA, USA, 2004; pp. 307–310. ISBN 978-0-306-47294-7.
66. Bott, A. A Positive Definite Advection Scheme Obtained by Nonlinear Renormalization of the Advective Fluxes. *Mon. Weather Rev.* **1989**, *117*, 1006–1016. [CrossRef]
67. Nenes, A.; Pandis, S.N.; Pilinis, C. ISORROPIA: A New Thermodynamic Equilibrium Model for Multiphase Multicomponent Inorganic Aerosols. *Aquat. Geochem.* **1998**, *4*, 123–152. [CrossRef]
68. Fountoukis, C.; Nenes, A.; Sullivan, A.; Weber, R.; Van Reken, T.; Fischer, M.; Matías, E.; Moya, M.; Farmer, D.; Cohen, R.C. Thermodynamic Characterization of Mexico City Aerosol during MILAGRO 2006. *Atmos. Chem. Phys.* **2009**, *9*, 2141–2156. [CrossRef]
69. Schell, B.; Ackermann, I.J.; Hass, H.; Binkowski, F.S.; Ebel, A. Modeling the Formation of Secondary Organic Aerosol within a Comprehensive Air Quality Model System. *J. Geophys. Res. Atmospheres* **2001**, *106*, 28275–28293. [CrossRef]
70. Strader, R.; Lurmann, F.; Pandis, S.N. Evaluation of Secondary Organic Aerosol Formation in Winter. *Atmos. Environ.* **1999**, *33*, 4849–4863. [CrossRef]
71. EMEP/EEA Air Pollutant Emission Inventory Guidebook—2016—European Environment Agency. Available online: https://www.eea.europa.eu/publications/emep-eea-guidebook-2016 (accessed on 24 January 2023).
72. EMEP/EEA Air Pollutant Emission Inventory Guidebook 2019—European Environment Agency. Available online: https://www.eea.europa.eu/publications/emep-eea-guidebook-2019 (accessed on 24 January 2023).
73. Inemar (Inemar.WebHome)—XWiki. Available online: https://www.inemar.eu/xwiki/bin/view/Inemar/WebHome (accessed on 24 January 2023).
74. Guenther, A.B.; Jiang, X.; Heald, C.L.; Sakulyanontvittaya, T.; Duhl, T.; Emmons, L.K.; Wang, X. The Model of Emissions of Gases and Aerosols from Nature Version 2.1 (MEGAN2.1): An Extended and Updated Framework for Modeling Biogenic Emissions. *Geosci. Model Dev.* **2012**, *5*, 1471–1492. [CrossRef]
75. Bigi, A.; Ghermandi, G.; Harrison, R.M. Analysis of the Air Pollution Climate at a Background Site in the Po Valley. *J. Environ. Monit.* **2012**, *14*, 552–563. [CrossRef]
76. Ramacher, M.O.P.; Karl, M.; Bieser, J.; Jalkanen, J.-P.; Johansson, L. Urban Population Exposure to NO_x Emissions from Local Shipping in Three Baltic Sea Harbour Cities—A Generic Approach. *Atmos. Chem. Phys.* **2019**, *19*, 9153–9179. [CrossRef]
77. Ghermandi, G.; Fabbi, S.; Veratti, G.; Bigi, A.; Teggi, S. Estimate of Secondary NO2 Levels at Two Urban Traffic Sites Using Observations and Modelling. *Sustainability* **2020**, *12*, 7897. [CrossRef]
78. Gsella, A.; de Meij, A.; Kerschbaumer, A.; Reimer, E.; Thunis, P.; Cuvelier, C. Evaluation of MM5, WRF and TRAMPER Meteorology over the Complex Terrain of the Po Valley, Italy. *Atmos. Environ.* **2014**, *89*, 797–806. [CrossRef]
79. Veratti, G.; Fabbi, S.; Bigi, A.; Lupascu, A.; Tinarelli, G.; Teggi, S.; Brusasca, G.; Butler, T.M.; Ghermandi, G. Towards the Coupling of a Chemical Transport Model with a Micro-Scale Lagrangian Modelling System for Evaluation of Urban NOx Levels in a European Hotspot. *Atmos. Environ.* **2020**, *223*, 117285. [CrossRef]
80. Paglione, M.; Gilardoni, S.; Rinaldi, M.; Decesari, S.; Zanca, N.; Sandrini, S.; Giulianelli, L.; Bacco, D.; Ferrari, S.; Poluzzi, V.; et al. The Impact of Biomass Burning and Aqueous-Phase Processing on Air Quality: A Multi-Year Source Apportionment Study in the Po Valley, Italy. *Atmos. Chem. Phys.* **2020**, *20*, 1233–1254. [CrossRef]
81. Brege, M.; Paglione, M.; Gilardoni, S.; Decesari, S.; Facchini, M.C.; Mazzoleni, L.R. Molecular Insights on Aging and Aqueous-Phase Processing from Ambient Biomass Burning Emissions-Influenced Po Valley Fog and Aerosol. *Atmos. Chem. Phys.* **2018**, *18*, 13197–13214. [CrossRef]
82. Hakimzadeh, M.; Soleimanian, E.; Mousavi, A.; Borgini, A.; De Marco, C.; Ruprecht, A.A.; Sioutas, C. The Impact of Biomass Burning on the Oxidative Potential of $PM_{2.5}$ in the Metropolitan Area of Milan. *Atmos. Environ.* **2020**, *224*, 117328. [CrossRef]
83. Vautard, R.; Builtjes, P.H.J.; Thunis, P.; Cuvelier, C.; Bedogni, M.; Bessagnet, B.; Honoré, C.; Moussiopoulos, N.; Pirovano, G.; Schaap, M.; et al. Evaluation and Intercomparison of Ozone and PM10 Simulations by Several Chemistry Transport Models over Four European Cities within the CityDelta Project. *Atmos. Environ.* **2007**, *41*, 173–188. [CrossRef]
84. Solazzo, E.; Bianconi, R.; Pirovano, G.; Matthias, V.; Vautard, R.; Moran, M.D.; Wyat Appel, K.; Bessagnet, B.; Brandt, J.; Christensen, J.H.; et al. Operational Model Evaluation for Particulate Matter in Europe and North America in the Context of AQMEII. *Atmos. Environ.* **2012**, *53*, 75–92. [CrossRef]
85. Pirovano, G.; Colombi, C.; Balzarini, A.; Riva, G.M.; Gianelle, V.; Lonati, G. PM2.5 Source Apportionment in Lombardy (Italy): Comparison of Receptor and Chemistry-Transport Modelling Results. *Atmos. Environ.* **2015**, *106*, 56–70. [CrossRef]
86. Thunis, P.; Pederzoli, A.; Pernigotti, D. Performance Criteria to Evaluate Air Quality Modeling Applications. *Atmos. Environ.* **2012**, *59*, 476–482. [CrossRef]
87. Pernigotti, D.; Gerboles, M.; Belis, C.A.; Thunis, P. Model Quality Objectives Based on Measurement Uncertainty. Part II: NO2 and PM10. *Atmos. Environ.* **2013**, *79*, 869–878. [CrossRef]
88. Pernigotti, D.; Thunis, P.; Cuvelier, C.; Georgieva, E.; Gsella, A.; De Meij, A.; Pirovano, G.; Balzarini, A.; Riva, G.M.; Carnevale, C.; et al. POMI: A Model Inter-Comparison Exercise over the Po Valley. *Air Qual. Atmos. Health* **2013**, *6*, 701–715. [CrossRef]
89. Thunis, P.; Clappier, A.; Pisoni, E.; Degraeuwe, B. Quantification of Non-Linearities as a Function of Time Averaging in Regional Air Quality Modeling Applications. *Atmos. Environ.* **2015**, *103*, 263–275. [CrossRef]

90. Carnevale, C.; Pisoni, E.; Volta, M. A Non-Linear Analysis to Detect the Origin of PM_{10} Concentrations in Northern Italy. *Sci. Total Environ.* **2010**, *409*, 182–191. [CrossRef]
91. Bessagnet, B.; Beauchamp, M.; Guerreiro, C.; de Leeuw, F.; Tsyro, S.; Colette, A.; Meleux, F.; Rouïl, L.; Ruyssenaars, P.; Sauter, F.; et al. Can Further Mitigation of Ammonia Emissions Reduce Exceedances of Particulate Matter Air Quality Standards? *Environ. Sci. Policy* **2014**, *44*, 149–163. [CrossRef]